

FOG

Freiberg Online Geoscience

FOG is an electronic journal registered under ISSN 1434-7512



2015, Volume 41



Broder Merkel & Mandy Hoyer (Eds.)

FOG special volume: Groundwater supply in the Middle East – three case studies from Syria, Iraq and Palestine

64 pages, 3 contributions

List of contents

Abo, R.; Merkel, B.: Hydrostratigraphic modeling of the central and southwestern part of Aleppo basin, Al Zebra catchment area, Syria	1
Jassas, H.; Kanoua, W.; Merkel, B.: Modeling groundwater flow in Aqra Plain unconfined aquifer, north of Iraq	33
Sabri, R.; Merkel, B. ; Tichomirowa, M.: Has the water supply network of Sebestia been connected to that of Nablus?	46

The pictures on the cover page have been taken by Raghid Sabri in 2011 during her field work in Palestine. They show the following features:

- Upper left corner: Aqueduct Beit Iba
- Upper right corner: Rehabilitated spring house, Qaryon
- Bottom left corner: Tunnel dewatering Harun spring
- Bottom right corner: Tunnel dewatering Subyan spring

Hydrostratigraphic modeling of the central and southwestern part of Aleppo basin, Al Zebra catchment area, Syria

Abo, Rudy

Department of Hydrogeology, Institute of Geology, Technische Universität Bergakademie Freiberg, Gustav-Zeuner-Str. 12, 09599 Freiberg, Germany; email: rudy.abo@hotmail.de

Merkel, Broder

Department of Hydrogeology, Institute of Geology, Technische Universität Bergakademie Freiberg, Gustav-Zeuner-Str. 12, 09599 Freiberg, Germany; email: merkel@geo.tu-freiberg.de

Abstract: Groundwater is the main source of drinking and irrigation water in most arid and semi-arid countries. In such environments, management of water resources is the key challenge for sustainable development projects. Aleppo basin is not an exception, the accelerated socio-economic development in that region has considerably increased the demand for water. Consequently, a significant degradation of the groundwater levels has been observed over the last three decades. The objectives of this study are to investigate the hydrogeological flow regime and water budget in the central and southwestern part of Aleppo basin, including the construction of three-dimensional lithological and hydrostratigraphic models for better understanding the nature and distribution of aquifer systems in the study area. The study also investigates the relationship between the geophysical records of normal-resistivity and the aquifers' hydraulic permeability. Visual MODFLOW with MODFLOW-NWT and ZoneBudget packages were used to simulate steady-state groundwater flow and water budget of the Neogene and Paleogene aquifers. The results show a significant relationship between the normal-resistivity of the hosting formations and the aquifers' hydraulic permeability, suggesting that the two fitted models in the region with an R^2 of 96.96 and 98.95% and P-values of 0.0001 and 0.0005 are suitable for depicting the Neogene and Paleogene aquifers, respectively. The calibrated groundwater heads show a general groundwater flow direction from the northern and northeastern to the southern and southwestern parts of the catchment, with an average drawdown ranging from 0.6 to 4 m for the first and the second aquifer, respectively. The study also shows an average groundwater recharge of 5 mm/year for the central parts of the catchment and 15-30 mm/year over the highlands (Al Hass and Jebel Simon), and a significant contribution of surface water to the total inflow in the upper aquifer as focused recharge. The simulated water leakage from the river to the upper aquifer is estimated as 3466.3 m³/day. Sensitivity analysis shows that both hydraulic conductivity and groundwater recharge are the main factors controlling the groundwater flow regime.

Keywords: 3-D geological model, conceptual model, groundwater model, MODFLOW WNT, RockWorks

1 Introduction

Groundwater resource management requires adequate information about the geological frameworks and hydrogeological system of the modeled region. These include a detailed description of the lithology and stratigraphic units, a good understanding of the tectonics and structural development, and initial information about groundwater flow within different layers. The petrological constitution of the rocks has direct impacts on the hydrogeological properties of geological formations. Slight changes in the petrography can have significant effects on the rocks' density and compressibility, the ratio of effective to total porosity, the hydraulic conductivity and thus the formation storativity (specific storage, specific yield), and consequently the ability of groundwater to flux in the unsaturated or saturated hydrostratigraphic units.

Generally, most of these changes cannot be observed directly. Therefore, geological and hydrogeological modeling is helpful to simulate and understand different subsurface physical and chemical processes. The more accurate the geologic model, the better its analytical capabilities, and thus the more detailed the maps and models that can be deduced (Berg et al. 2009). Building a conceptual model of an area helps to simplify the field problems so that the system can be analyzed more efficiently (Anderson and Woessner 1992). However, before starting to build a groundwater model, it is essential to create lithological and stratigraphic models of the area, providing information about the formation's textures, rock materials, strata thickness, ages, and spatial variation in physical properties over the region of interest (Stone 1999).

Additionally, structural data and changes in the strata due to paleo- or new tectonic processes such as folds, joints, and faults are also very important and need to be considered during the modeling of the groundwater system. This information can be obtained from previously conducted geological and hydrogeological surveys, professional organizations, and published and unpublished reports in addition to the surface and subsurface geological tools (maps, cores, and logs from drilled boreholes). Lithology provides valuable information about the dominant rock types in the region and their physical and geochemical properties. It can also deliver important information to predict the origin of groundwater and the paleo-depositional environment (Davidson et al. 1997; Thompson and Turk 1998; Peng and Zhang 2007). The influence of rock lithology on the development of the drainage network and the basin shape was reported by Mukherjee and Jha (2011). Olvmo and Johansson (2002) investigated the impact of lithology on the degree of weathering and erosion of rock surfaces. Furthermore, rock lithology controls the response of rocks to the metamorphism and tectonic activity (Reed 1962) and affects groundwater movement in geological formations (Freeze and Cherry 1979; Anderson and Woessner 1992; Stone 1999; Pinder and Celia 2006; Hyndman et al. 2013).

A lithological model can provide a general overview of the spatial distribution of the main geological formations in a region. Furthermore, it facilitates more accurate discrimination of different stratigraphic units vertically and thus a more realistic conceptual groundwater model. In the last four decades, several techniques have been developed to predict rock lithology, such as seismic data interpretation (Doyen et al. 1988; Alkhalifah and Rampton 2001; Bachrach et al. 2003), physical well logs and geochemical data (Busch et al. 1987; Wendlandt and Bhuyan 1990; Fung et al. 1997), and, recently, remote sensing data (Rowan and Mars 2003; Ninomiya et al. 2005).

The software development in the last decades have provided powerful tools to build and visualize 3D-models at different resolutions in a reasonable time, delivering comprehensive information about the subsurface even in areas with complex geology. Subsurface modeling includes two main stages: the *conceptualization stage* (building the initial conceptual model) and the *model transformation stage* (converting all spatial and physical parameters into a numerical model). Similarly, groundwater models are able to solve diverse hydrogeological issues concerning flow prediction, contamination transport, surface and groundwater interaction, water balance, and seawater intrusion. These models differ in terms of geometry (1-D, 2-D, or 3-D groundwater models) as well as in the main approach (physical, analytical, or numerical models) (Anderson and Woessner 1992).

Generally, there are two main types of numerical methods that differ from each other in the mathematical concepts and the shapes of grid cells: the finite-difference method (rectangular grid; governing equations are solved by differentiation), and the finite-element method (mesh and irregular shapes;

solved by integration) (Stone 1999). However, the groundwater flow governing equation in 3-D can be written as follows:

$$\frac{\partial}{\partial x} \left(K_x \frac{\partial h}{\partial x} \right) + \frac{\partial}{\partial y} \left(K_y \frac{\partial h}{\partial y} \right) + \frac{\partial}{\partial z} \left(K_z \frac{\partial h}{\partial z} \right) = S_s \frac{\partial h}{\partial t} - R \quad (1)$$

where K_x , K_y , and K_z are the hydraulic conductivity in three dimensions, S_s is the specific storage, and R is the inflow volume into the system. The equation above can be solved analytically in one or two dimensions, but it is difficult to solve in the 3-D space with heterogeneous flow. Therefore, computer programs and codes are used to solve flow complexity under different conditions.

One of the programs widely used to model groundwater flow is the MODFLOW code developed by the US Geological Survey (USGS) and officially released in 1988 under the name of MODFLOW-88 (McDonald and Harbaugh 1988). The program was written in Fortran 66 programming language as a standard 3-D finite-difference groundwater flow modeling code of the USGS (McDonald et al. 2003). Recently, MODFLOW has been replaced by its advanced derivatives codes (MODFLOW-2000, MODFLOW-2005, and MODFLOW NWT) and other related packages (MODPATH, MT3D, and MT3DMS). These packages have been integrated in almost all commercial and public groundwater modeling software using very friendly graphical user interfaces (GUIs) (Chiang and Chiang 2001).

As mentioned above, both 3-D geological and hydrogeological models are essential to develop policies for groundwater resource management and sustainability projects, particularly in arid and semi-arid regions where water scarcity, drought, and developing infrastructure are the main challenges. Syria is a semi-arid country with limited water resources and accelerated population growth (about 19.5 million inhabitants in 2006).

According to the governmental report of the German Federal Institute for Geosciences and Natural Resources and the Syrian Ministry of Irrigation (BGR and MOI 2004), Syria is sub-divided into seven water resource basins. The Orontes and the Euphrates rivers are the main surface water storage in the country, with average flows of 13 to 210 m³/s, respectively.

The climate is Mediterranean with a cool winter and relatively long dry summers. The average annual precipitation in the country is 250 mm. As a traditional developing country, agriculture is one of the most important productive sectors in Syria. The actual area of cultivated land was about 5.95 million ha in 2006 (32 % of the total area of the country) (IFAD 2010). Thus, about 90 % of the water resources in Syria are used in irrigation and the remaining 10 % for domestic use and industrial purposes.

About 23 % of the total population of Syria live in the area of Aleppo basin. The region receives the majority of its water from Al Assad Lake on the Euphrates River and groundwater abstraction in the rural areas. Nevertheless, the city loses a significant amount of its water supply by illegal abstraction from groundwater with average loss reaches up to 35 % and physical leakage from water transporting canals varies from 20 to 40 % (BGR and MOI 2004). These facts raise concerns about water sustainability in the region. The aim of this study is to build 3-D hydrostratigraphic models for the main formations in the region of Al Zerba catchment, including detailed information about lithology, stratigraphy, and geophysical data. The study also aimed to construct a 3-D steady-state groundwater flow and balance models of the catchment area.

1.1 Characteristics of the study area

The catchment covers an area of approximately 573 km². It constitutes the southern and southwestern sites of Aleppo basin. The natural topographic boundaries are determined by the Al Hass Mountain in the east, Jebel Simon in the north, and Tel Hadya in the south. Al Qweek valley occupies the central part of the region. It expands to southern sites of the Aleppo basin and forms Al Matah depression (Fig. 1). The terrain of the study area is mostly flat (average slopes ≤ 7 %) with an average elevation ranging from 290 to 420 m above sea level (masl). Aleppo basin has a Mediterranean climate with

continental influence. This is manifested by a long hot summer (from April to October) and low humidity levels (< 30 %). The air temperature reaches up to 35°C during July and August (BGR and MOI 2004). According to UNEP (1997), the study area is characterized by semi-arid climate, with a potential pan evapotranspiration (*PET*) ranging from 1,200 to 1,400 mm/a and average precipitation of 350 mm. The average minimum and maximum annual temperature are 12 and 24°C, respectively.

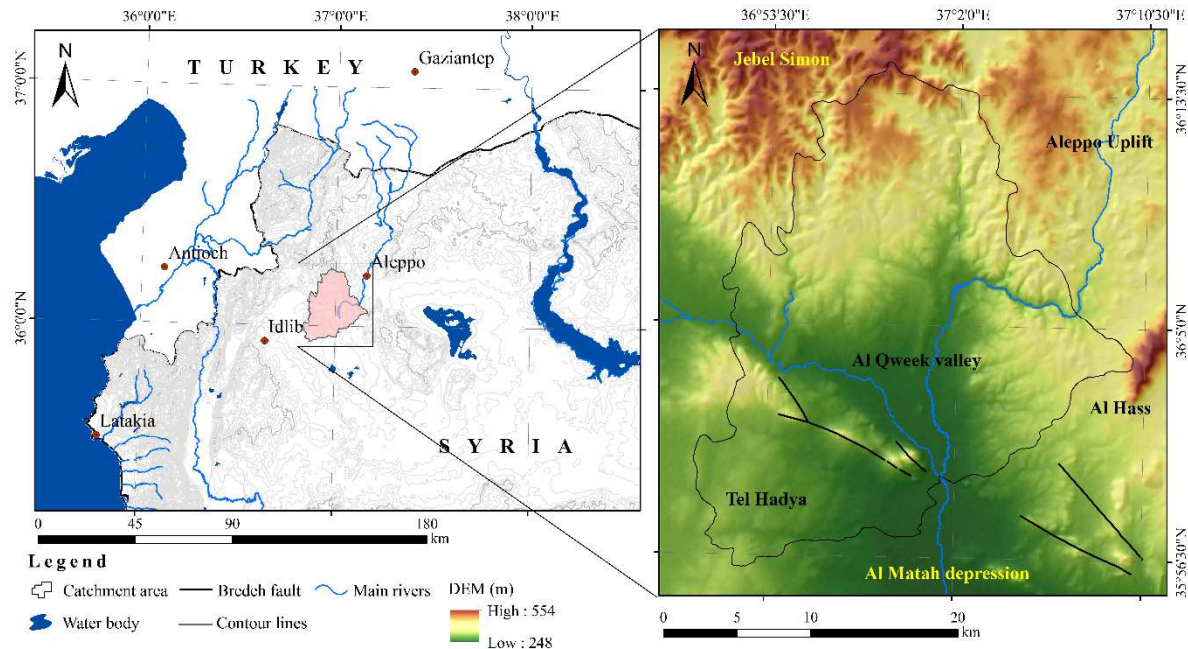


Fig. 1: Location of the study area (elevation data are provided by USGS SRTM 90 v2)

1.2 Geological setting

The geology of Aleppo basin is described by several reports and geological maps. The most recent geological survey was conducted by Soviet experts of Selkhozpromexport (1979) under the general guidance of V.P. Ponikarov, including hydrogeological and hydrological investigations in different areas of Syria. According to the geological survey at a scale of 1:200,000 (Ponikarov 1964) and data from deep boreholes (Fig. 3), a significant thickness of the Cretaceous deposits can be distinguished in the different sections of Aleppo basin, particularly in the western and southern parts of the basin.

The Campanian (K_2cp) and Maastrichtian (K_2m) stages crop out in the southern and western portions of Aleppo plateau with an average thickness of 300 m. They are located at depths ranging from 360 to 400 m in the northern part (Aleppo uplift) and a depth of about 130 m in the southern part of the study area (Tel Hadya). The Campanian deposits are mainly determined by dolomitized limestone with sets of flint and local interlayers of phosphorite, while alternations of clayey limestone and marl are lithologically the major deposits in the Maastrichtian stage.

Cretaceous formations were considered to be deposited in a relatively stable tectonic environment (Chaimov et al. 1990). However, Neogene deposits of the Helvetian stage (N_1h) are the most dominant outcropped formation in the northern and neighboring areas (Jebel Simon and Tel Hadya). They unconformably overlie the middle and upper Eocene (Pg_2^{2+3}), indicating a new marine transgression (Zanchi et al. 2002). In Al-Matah depression, Helvetian deposits are covered by a good thickness of Quaternary sediments (Pleistocene). In all sections of the geological map, Helvetian limestone is essentially characterized by an aphanitic structure and a karstified alternation of conglomerates, sandy limestones, and marls. The total thickness ranges between 80 and 300 m.

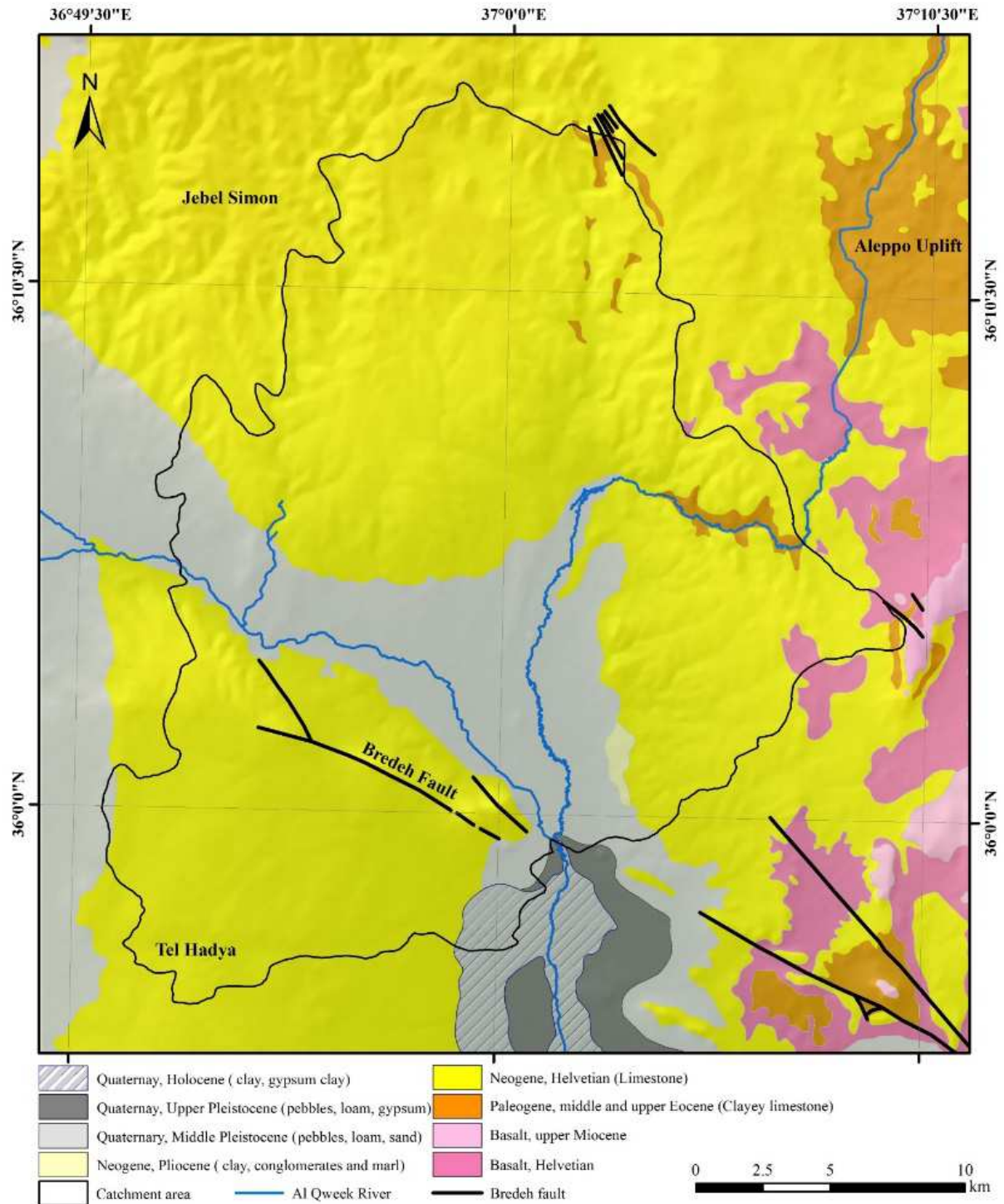


Fig. 2: Simplified geological map according to Ponikarov (1964)

The Helvetian and upper Miocene basalts are also widely distributed in the eastern parts of the study area and cover considerable areas of Jebel Al Hass and southern parts of Aleppo uplift. Massive basalts can be found in the highlands, interbedded with limestones and covered with red clay on the fringes of Al Qweek valley. The reported average thickness ranges from 10 to 50 m (Selkhozpromexport 1979). The deposits of the middle and upper Eocene can be seen over the northeastern sites of the study area (Aleppo city) and locally as small outcrops in the riverbed of Al Qweek River and Jebel Simon in the north. They mainly consist of clayey and silicified limestone and nummulitic limestones with alternation of marls and clayey limestones containing thin flint. According to the data of the deep boreholes, the stratum thickness ranges from 100 m in the central areas to 340 m in the Aleppo uplift.

Quaternary sediments in the region belong to the Pleistocene and Holocene stages (Q_3 and Q_4), and have significant thicknesses, particularly in the interior parts of the catchment area. They are confined by Al Qweek valley and Al Matah depression in the south and consist of lacustrine proluvial and alluvial deposits. The lacustrine deposits of the upper Pleistocene and Holocene have an average thickness of 5–10 m in Al Matah depression and consist mainly of pebbles and heavily gypsified clays (Selkhozpromexport 1979; Gruzgiprovodkhoz 1982). The tectonics of Al Zerba region is characterized by a group of folds with a SE–NW strike direction occurring in all stratigraphic sequences of Aleppo plateau. The area forms a sequence of anticlines of Neogene and Paleogene successions (Al Hass, Jebel Simon anticlines) confining Khanasser, Al Matah, and Afrin synclines, which are filled with Quaternary sediments. Ponikarov (1964) identified Al Bredeh strike slip fault, which crosses the study area with a strike direction of SE–NW (approx. $E 120^\circ W$). According to the structural analysis conducted by Zanchi et al. (2002), the fault region is dominated by systematic joints transversal to the folds with E–W trending axes in the south, suggesting a N–S compression.

1.3 Hydrogeology and regional aquifers

Aleppo basin was extensively investigated by (Wolfart 1966), (Selkhozpromexport 1979), (Gruzgiprovodkhoz 1982), (JICA 1997), (UN-ESCWA 1997), (GCHS 1999), and (BGR and MOI 2004). The hydrogeological system of Aleppo basin is determined by three main aquifer systems from the bottom to the top (UN-ESCWA 1997; ICARDA 2000). The deep Cretaceous aquifer is identified by dolomitized limestone (Cenomanian/Turonian) and located at an average depth of 400 m, while its average thickness ranges from 250 to 350 m (Table 1). This aquifer is confined by the Maastrichtian marl and clay deposits in the top. It bears brackish to saline groundwater with high sulfate content (Gruzgiprovodkhoz 1982). The middle aquifer is unconfined and determined by the Paleogene (Eocene) deposits. It covers considerable areas in the western and southern parts of Al Matah depression. Water-bearing rocks are determined by chalky and clayey limestone with average thickness varying from 100 m in the south to 320 m in the northeastern parts of the catchment. This formation is overlain by Helvetian limestone (upper aquifer) and interbedded with basalts to the east, with an average thickness of 120 m, as shown in Fig. 3.

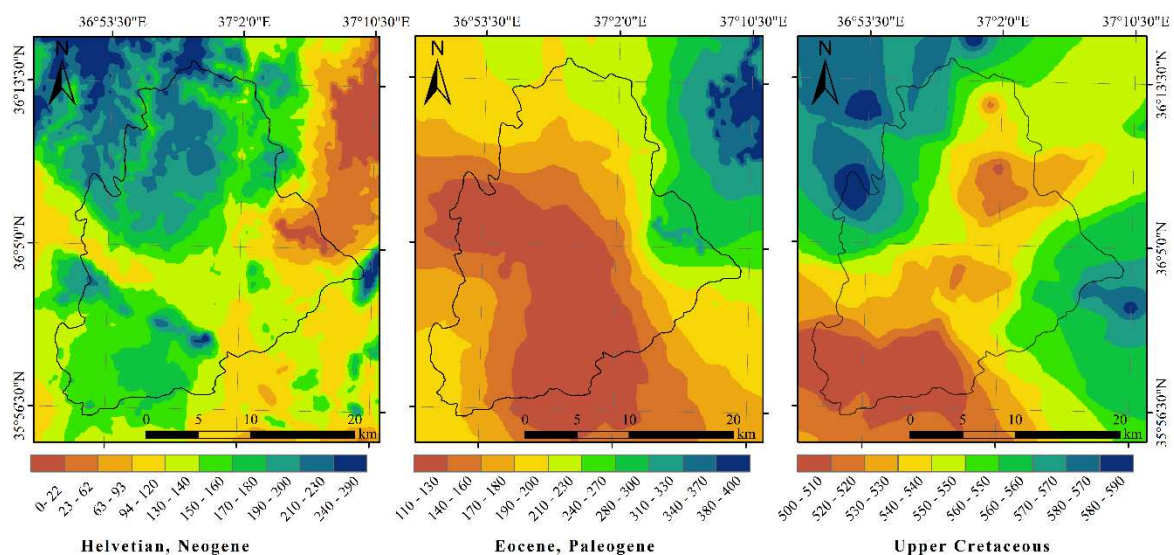


Fig. 3: Stratigraphic thickness in meters (isopach) of the three major aquifers in the catchment area

According to the piezometric surfaces of the upper and middle aquifers, the groundwater of the upper aquifer flows from the east (Al Hass Mountain) to the southwestern sites of the catchment, with a general decrease in the hydrostatic pressure from 345 to 190 m, while groundwater flows from the eastern to the western sites for the middle aquifer with a lower hydraulic difference of 15 to 20 m (Fig. 4).

Both aquifers are considered to be recharged by direct and indirect infiltration of precipitation and lateral inflow of groundwater from adjacent horizons along the eastern and southern edges (Gruzgiprovodkhoz 1982). The average potential groundwater recharge of the region ranges from 10 to 60 mm/a according to Wolfart (1966), Gruzgiprovodkhoz (1982), JICA (1997), Martin (1999), Luijendijk (2003), Luijendijk and Bruggeman (2008), and Abo and Merkel (2015). Furthermore, as a result of hydrochemical investigation of stable isotopes (^{18}O and ^2H), (Stadler et al. 2012) proposed the Helvetian limestone outcrops as a past and present groundwater recharge area.

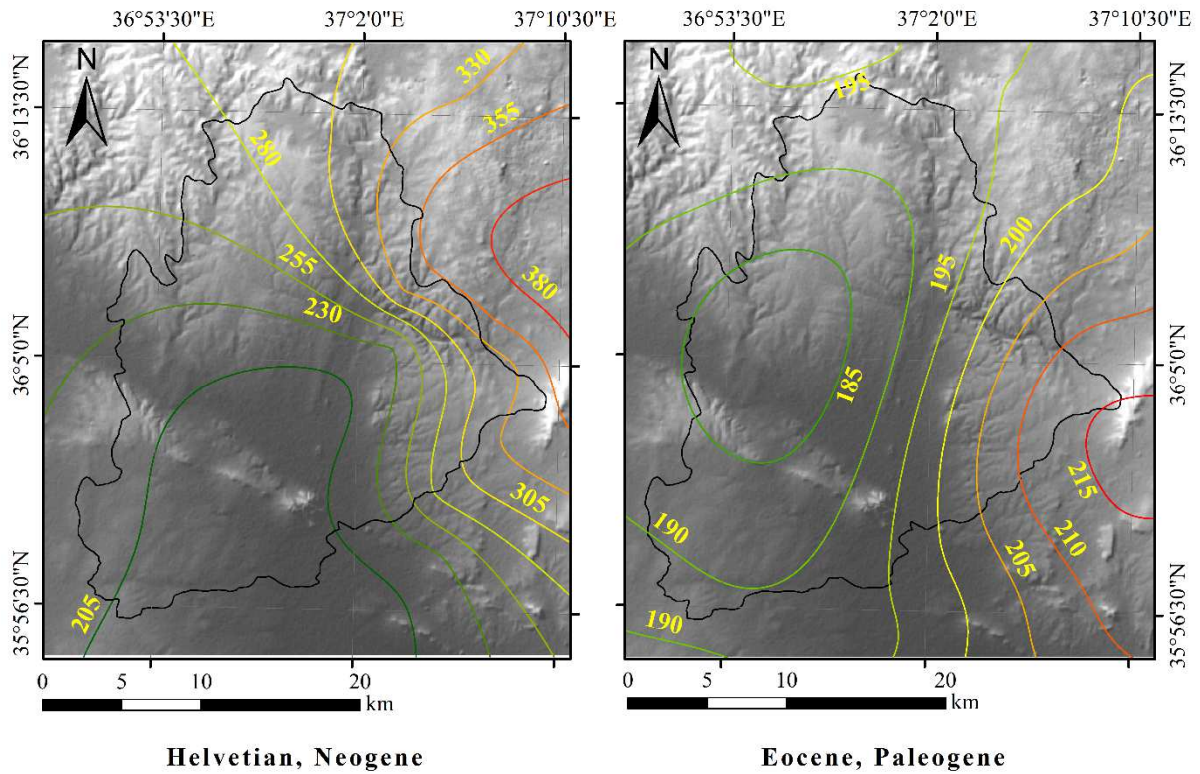


Fig. 4: The interpolated hydro-isohypse of the upper (Helvetian) and middle aquifer (Eocene) based on the observation of groundwater static level for the period 2001-2010

2 Materials and methods

2.1 Datasets

A total of 30 deep boreholes were used for the lithological and stratigraphic modeling, including the detailed description of the lithology, depths, ages, and geophysical records (gamma ray and normal-resistivity logs). Figure 5 shows the locations and total depths of the selected boreholes. The total depths of the boreholes range from 200 to 875 m. They fully penetrate the Neogene and Paleogene and partly penetrate the Upper Cretaceous. All borehole data was provided by the Syrian Ministry of Irrigation (MOI) and the General Company of Hydraulic Studies (GCHS). Additionally, the 1:200,000 geological map of Ponikarov (1964) and sections at different scales were used to calibrate the final models.

The geological modeling was performed using the RockWorks software packages (RockWare Inc 2010), while ESRI ArcGIS version 10.1 (ESRI Inc 2011) was used for the post-processing of spatial data. The RockWorks program uses different types of algorithms to interpolate the 3-D distribution of the geological units. As a consequence the results would not simulate the actual distribution of outcrops in reality. Therefore, 45 virtual boreholes were integrated into the model database to wrap the outcropped formations to simulate the geological surface. Moreover, the digital geological map (polygon files), formation boundaries, and lineaments (polylines) were used to calibrate the final model.

On the other hand, the 1:200,000 hydrogeological map (Gruzgiprovodkhoz 1979), aquifer thicknesses, horizon grid files, and aquifer hydraulic properties (hydraulic conductivity K , specific yield S_y , specific storage S_s , and transmissivity T) were used to construct the groundwater conceptual model of the catchment area. The 3-D hydrogeological simulation was carried out using Schlumberger Visual MODFLOW version 4.6 (Schlumberger 2010). The hydraulic information of Al Qweek River and the groundwater initial head, constant head, evaporation, groundwater abstraction and recharge boundary conditions were used in the simulation. The groundwater heads were calibrated using 20 groundwater observation wells. Figure 6 shows the locations of the observation and pumping wells in the region.

Tab. 1: The sequence of the aquifer system in the Aleppo basin according to UN-ESCWA (1997) and ICARDA (2000)

Stratigraphic Age		Aquifers	Hydrogeological Significance	Lithology	Thickness (m)	Salinity	Water Type		
Quaternary	Holocene	Upper	Aquifer with low productivity and limited extent and/or that is discontinuous	Gypsum-salinized loam, sand to pebbly proluvium and alluvial sediments	10–50	Fresh to Brackish	Ca-Na-SO ₄ -Cl		
	Pleistocene								
Neogene	Pliocene			Basalt	> 50	Fresh	Ca-HCO ₃		
				Calcareous sandstone	30–50	Fresh	Ca-HCO ₃		
	Messinian			Basalt	5–30	N/a	N/a*		
	Miocene			Tortonian	Local perched aquifers	Gravel, marl, limestone	10–20	N/a	Ca-HCO ₃
				Helvetian	Upper aquifer with high productivity	Limestone, fissured, karstified	5–50	Fresh	Ca-Mg-HCO ₃
Paleogene	Oligocene			Middle	Main upper aquifer (= middle aquifer) with medium productivity	Limestone, chalk, marly chalk	40–100	Fresh brackish	Ca-Mg-HCO ₃
									N/a
	Eocene				Middle	Local discontinuous aquifers with low productivity	Limestone, karstified	0–100	Fresh to brackish
		Lower	Aquitard		Marl, chalk, chert	0 – > 460	N/a	N/a	
Cretaceous	Upper	Lower	Main deep aquifer with high productivity	Limestone, dolomite, strongly fissured, karstified	250–350	Brackish	Ca-SO ₄ and Na-Cl [H ₂ S]		
							Maastrichtian		
							Campanian		
	Lower		Cenomanian	Aquitard	Marl	> 500	N/a	N/a	
			Albian						
			Aptian						

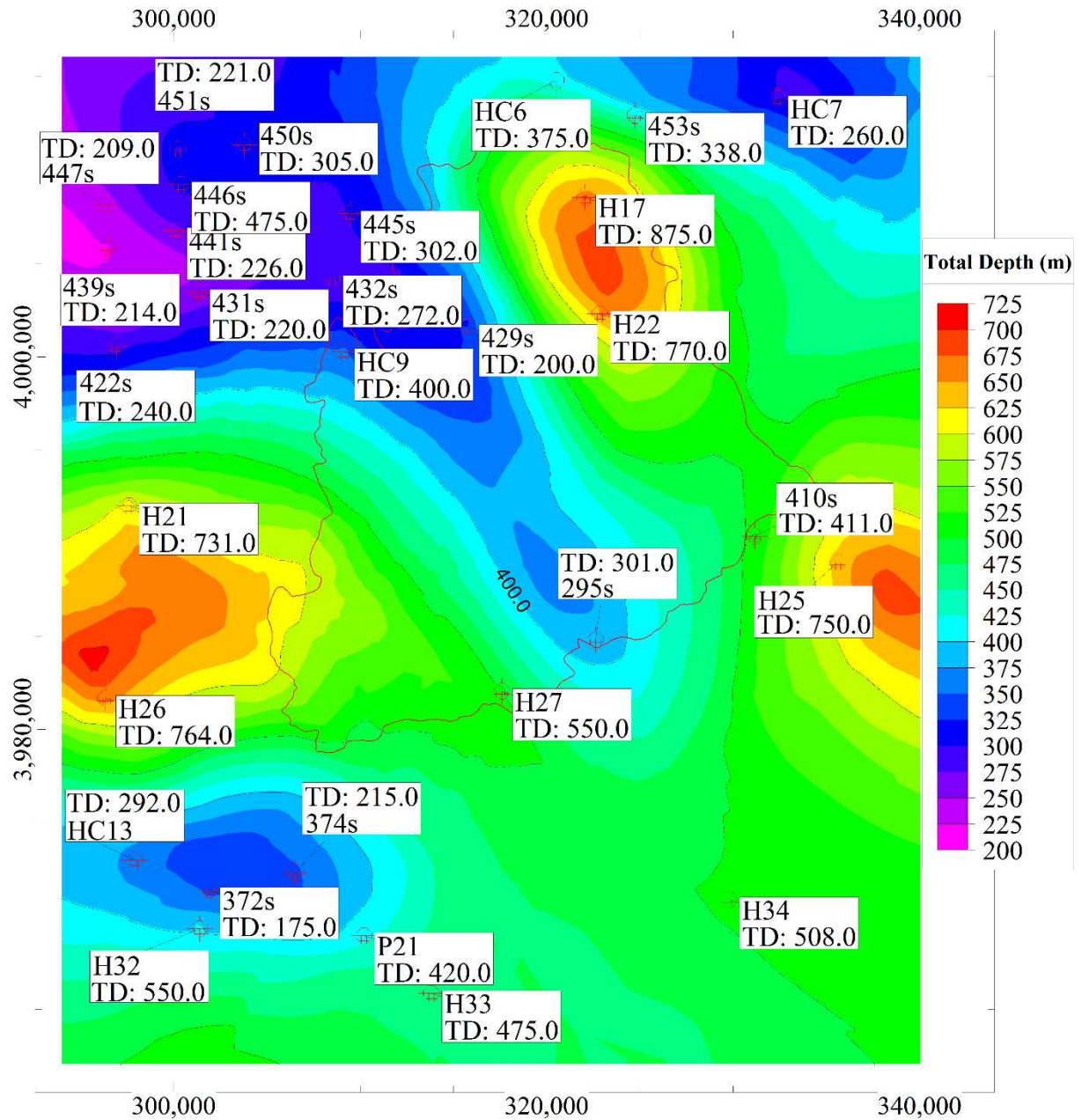


Fig. 5: The locations and total depths of the exploration boreholes

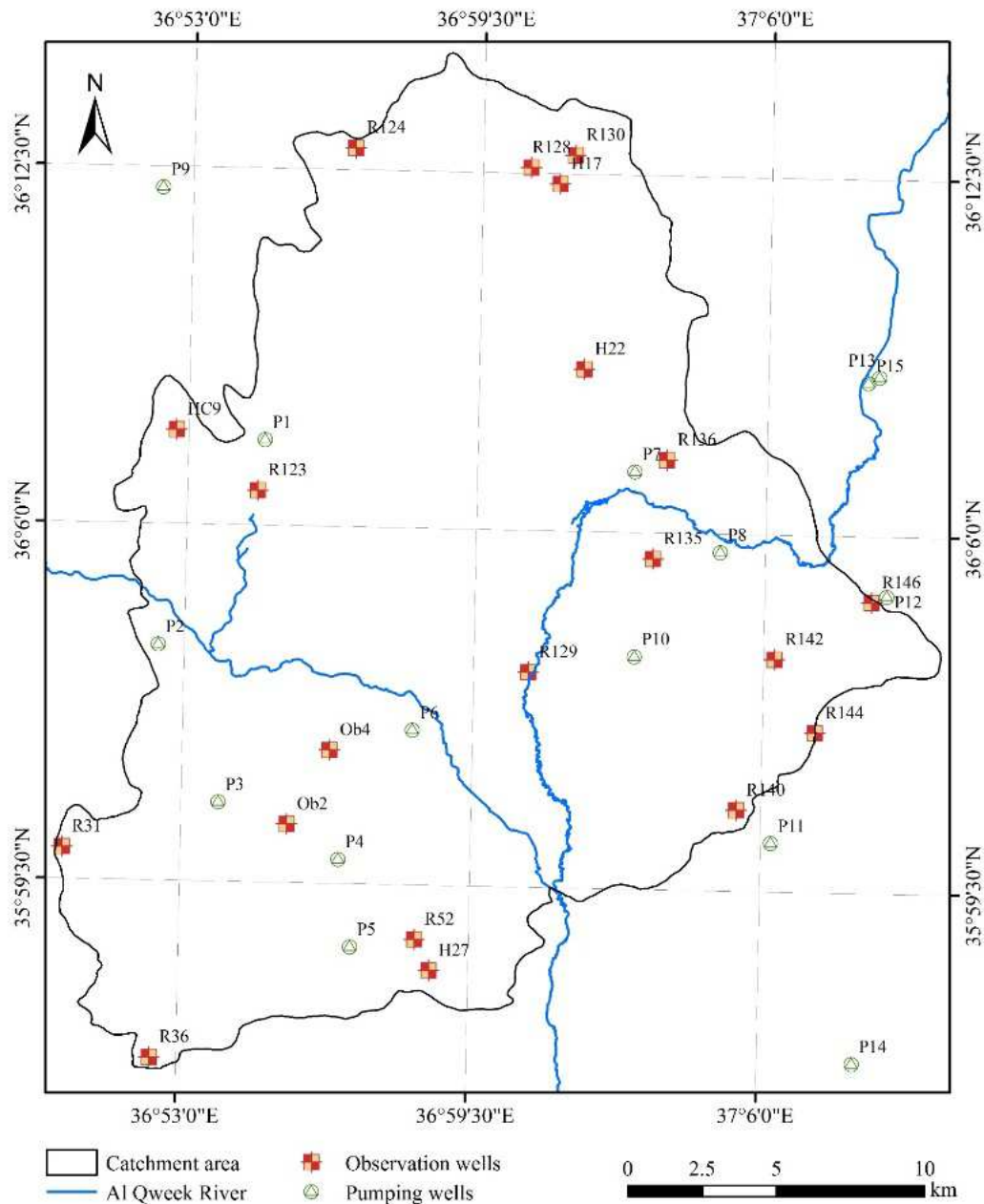


Fig. 6: The locations of observation and pumping wells

2.2 Data preparation

The lithological succession, ages, depths, elevations, and geophysical logging data were transformed into data sheets. The formations were subdivided into depths in dependence on their lithological types, estimated ages, core information, and gamma ray data. Resistivity and gamma ray records were resampled at fixed depths intervals of 0.5 m. After that, borehole data were imported into the RockWorks database, including all information on the model geometry, its coordinates, lithology, and stratigraphy as well as borehole logging data (*P-data*). Table 2 lists the main data integrated into the RockWorks model. Moreover, spatial information (shape files, surface geological boundary, and faults) were imported into the software and saved into the polyline/polygons database.

A digital elevation model (DEM) from Shuttle Radar Topographic Mission (STRM 90) of 90×90 m horizontal resolution was used to replicate the region's ground surface. The DEM was resampled to fit the horizontal and vertical resolution of the model using the "Grid/Math" tool in the RockWorks utilities. The output model dimensions were adjusted to 150×150 m and 9 m for the horizontal and verti-

cal spacing, respectively, with a total of 12,453,056 nodes and area of 2496.6 km². The model output minimum and maximum vertical dimensions were adjusted from –520 to 480 m.

Monthly groundwater observation data cover the years from 2001 to 2010, river hydraulic information and riverbed texture, the results of previous pumping tests (storativity and hydraulic conductivity), and well pumping data were organized into compatible Microsoft Excel spreadsheet format. These data were imported into ArcGIS and stored in the software database with other spatial data (catchment area, rivers, and well locations) as shape files.

Tab. 2: The input data of the lithological and stratigraphic models

<i>Data</i>	<i>Type</i>	<i>Details</i>	<i>source</i>
Boreholes	Coordinates, well position	UTM WGS 1984 zone 37N	
	Total depth	m	
	Well top elevation	m	
	Stratigraphic information	Age, composition-based discrimination	GCHS (Aleppo basin development project
	Lithological description	Rock composition	Phase II)
	Succession depths	m	
	Ages	Fossils/radiometric ages dating	
	Resistivity and gamma log	Vertical log records	
	Well construction	Casing, hole geometry	
Shape files	Geological boundaries		1:200,000 Geological map Ponikarov (1964)
	Lineaments	Digitization	

2.3 Lithological model

The lithology of the stratigraphic formation within the study area was described using a 3-D lithological model carried out using the *Lithology* modeling option of RockWorks. First the lithological types of different geological formations were identified from the lithological column of the selected boreholes and information obtained from gamma ray records. These were stored in the *Lithological Types* table in the RockWorks database. The table includes detailed information about rock material, pattern, color, and order in the model from the top to the base. The most important entry in the lithological types table is the numerical G-value, which represents the rock types, so each layer must have a certain G-value (RockWare Inc 2010). These values have been used to interpolate the lithology of different stored formations in the project database. Table 3 lists the distinguished lithological types of the region. The solid model was carried out using the borehole database (spatial information, depths, and lithological types). The lateral extrusions, advanced random midpoint correlations, and outlier interpolation algorithms were used in the full voxel mode modeling option available in RockWorks.

The *random midpoint algorithm* is very helpful for minimizing abrupt changes in the layers, providing more blending and a reasonable model. Furthermore, outlier interpolation assigns all model voxels to a defined G-value and excludes any outlying abnormal nodes as null values. The model was smoothed by 2×2 voxels (filter size) and constrained using the resampled DEM representing the model topographic surface. The warping option was also used in the modeling to bias the solid model with the topographic surface. In addition, the volume of each lithology type in the region was computed. The lithological sections and fence diagram were created based on the final reasonable constructed model. However, lithological modeling in RockWorks is a time-consuming process and depends on the model resolution and the performance of the interpolation and modeling unit (personal computer). The flowchart below summarizes the sequence of lithological modeling in RockWorks (Fig. 7).

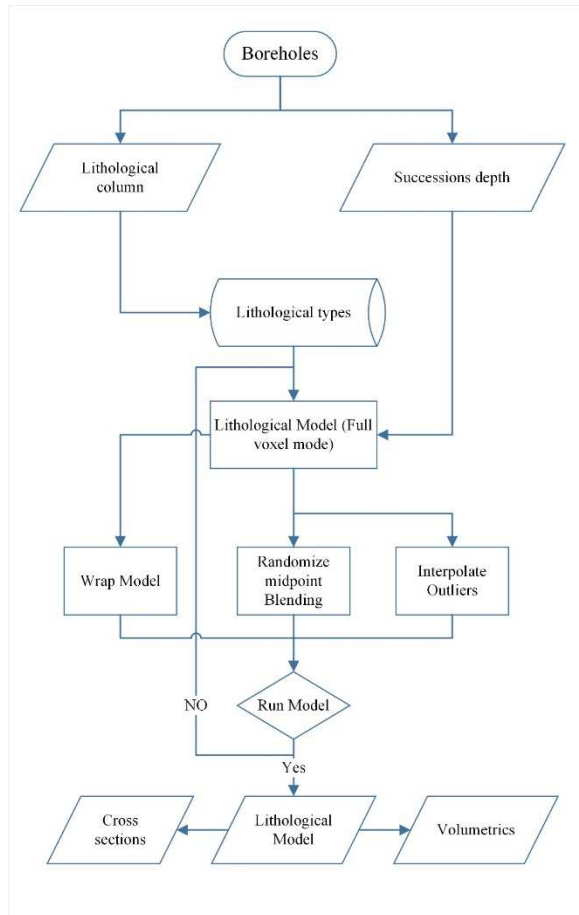


Fig. 7: Flowchart showing the main sequence of the lithological modeling using RockWorks

Tab. 3: The lithology types of the study area

<i>Lithological units</i>	<i>Description</i>	<i>Age</i>	<i>G-Value</i>	<i>Pattern</i>
Basalt	Massive basalt	Helvetian	6	
Quaternary sediments	Pebbles, loams, gypsum, and salty clays	Pleistocene	1	
Limestone	Limestone, conglomerates	Helvetian	2	
Clayey limestone	Limestone, clayey limestone, and flints	Middle and upper Eocene	3	
Marly limestone	Marls, marly limestone	Maastrichtian, Danian	4	
Dolomitized limestone	Dolomites, limestone, and flints	Cenomanian, Turonian	5	

2.4 Advanced stratigraphic modeling

The stratigraphic model of the study area was constructed from the boreholes by interpolating the top and base grid surfaces of each unit listed in the stratigraphic database. The stratigraphic successions of the study area were determined in terms of the relative ages of the geological formations and by four main units: the Quaternary, Neogene, Paleogene, and Upper Cretaceous (Maastrichtian/Danian) formations. Similarly to the lithological modeling, the stratigraphic types and G-values of the layers were assigned based on the borehole database. The inverse distance weighted (IDW) algorithm was used to

interpolate the top and bottom surfaces of each modeled stratum. Additionally, the declustering option was selected in order to reduce noise within the interpolated horizons. Moreover, these surfaces were smoothed by one filter size (each node is assigned the average of itself and the eight nodes surrounding it). The general form of the IDW algorithm is given by the following equation (Isaaks and Srivastava 1989; Bartier and Keller 1996):

$$p_{x,y} = \frac{\sum_{i=1}^n p_i w_i}{\sum_{i=1}^n w_i} \quad (2)$$

where $P_{x,y}$ is the estimated value of the grid node, P_i represents the control value at the location of sample point i , and w_i is the weighting function, which can be written as follows:

$$w_i = d_{x,y,i}^{-\beta} \quad (3)$$

where $d_{x,y,i}$ is the distance between $P_{x,y}$ and P_i , while β is the weighting power.

On the other hand, the topographic surface of the stratigraphic model was resampled to match the model resolution. Thin stratigraphic units with an average thickness close to 0 were removed by adjusting the thickness cutoff to zero. Ten stratigraphic modeling scenarios were created using different grid-resolution and interpolation options to optimize the stratigraphic model as far as possible. After that, the final reasonable model was modified using the advanced stratigraphic modeling procedure. This was performed using the *Grid* and *Grid Math* tool options in the RockWorks utilities. The thickness grids (isopach) were calculated by subtracting the top and base grids of the Neogene and Paleogene, applying the following equations:

$$Isopach_N = Top_N - Base_N \quad (4)$$

$$Isopach_{Pg} = Top_{Pg} - Base_{Pg} \quad (5)$$

where N is the Neogene and Pg the Paleogene layer. After that, the Quaternary grid files and Neogene and Paleogene thicknesses were clipped to their real geological boundaries as shown on the 1:200,000 geological map. To ensure convergence between all layers, the top and base horizons were reconstructed using the *Math/Grid to Grid* conversion tools based on the newly configured grid files. This was achieved by subtracting each stratum thickness from its lower surface to generate the top of the next formation below. Finally, the stratigraphic solid model was created using the modified horizons of outcropped formations.

2.5 Resistivity model and aquifer permeability

The resistivity of lithological formations varies within a wide range. Since most of the rocks mainly consist of minerals, some of them have insulation properties (Bell 2007). Moreover, the content of mineralized groundwater in porous rocks has a direct impact on the resistivity. The 3-D resistivity model of the study area was created using 13 deep boreholes with normal-resistivity logs. All record

data were imported into the RockWorks database and presented in ohm-meters (Ωm). After that, the solid model was constructed using the anisotropic inverse-distance (IDW-anisotropic) algorithm, which is essentially derived from the inverse-distance algorithm. This correction algorithm enables the program to look for the neighboring control points in each 90° sector round the node, particularly when observation points are not uniformly distributed (RockWare Inc 2010).

However, a voxel node value is given based on the weighted average of neighboring data points where the value of each data point is weighted according to the inverse of its distance from the voxel node, taken to a power (exponential inverse-distance). This method can improve interpolation of voxel values between different data clusters in the boreholes, but it is slower than other algorithms such as IDW-isotropic. Declustering, smoothing, supersurface, and warping layers were also performed in the modeling. After interpolation, the solid model was clipped to the catchment boundary. A north–south cross-section was created based on the model and integrated with gamma ray logs. After that, the average resistivities of both Neogene and Paleogene were interpolated and exported as raster layers into ArcGIS. The relationship between the aquifers' hydraulic conductivity of 12 boreholes and the average resistivity was also assessed. The boreholes were separated into two main groups: the Neogene boreholes (423s, 445s, 424s, 432s, 398s, and 387s) and the Paleogene ones (453s, 448s, 429s, H25, HC9, and H22) (Fig. 5). Each borehole represents a single value of average resistivity of the selected aquifer (intersection point of boreholes and average resistivity grid of an aquifer) and hydraulic conductance obtained from the previous results of pumping tests. After that, simple regression analysis was performed to explain the potential relationship between the normal-resistivities and aquifer permeabilities.

2.6 Groundwater conceptual model

The results of the stratigraphic model of the catchment area were used to build the groundwater conceptual model. These include the topographic surface, faults, and stratigraphic horizons of the Neogene and Paleogene formations. The Cretaceous layer was excluded from the recent study since it focused on the first two aquifer systems and the limitation of data concerning the deep aquifer. Inputs from different sources were used in the conceptual model, such as spatial data, shape files (rivers, boundary area), and observation and pumping wells.

All layers are referenced to the UTM WGS84 zone 37N projection system. The data were exported into the Hydro GeoBuilder software (Schlumberger 2009) to construct the conceptual model and transform it into a numerical model. Each type of data was stored in the conceptual workspace as an object (polyline, polygon, point, and surfaces). The conceptual structure model consists of three main horizons representing the geology of the region: the topographic surface, which is considered as an erosional surface, and the Neogene and Paleogene bases as conformable surfaces. The result is two structure zones which are used as property zones, so that each zone presents unique hydraulic properties (hydraulic conductivity, storativity, and initial heads). Figure 8 presents the general workflow of the conceptual model for the Al Zerba catchment area.

2.7 Groundwater model

The steady-state groundwater flow model was simulated using USGS MODFLOW-NWT code (Niswonger et al. 2011), which is a Newton-Raphson formulation for MODFLOW-2005 (Harbaugh 2005). The code was developed to improve the solution of unconfined groundwater flow problems such as dry cells distribution and rewetting nonlinearities. (Hunt and Feinstein 2012). However, the MODFLOW-NWT package in Visual MODFLOW includes two asymmetric matrix-solvers: the generalized-minimum-residual (GRMRES) and the stabilized conjugate gradient (CGSTAB) solver.

In this study, the GRMRES solver was used with a moderate nonlinear automate-solver option, which is important for a successful convergence in the case of nonlinear models with more than one unconfined aquifer. The model discretization was constructed as a 100×100 m grid spacing with 313 columns and 355 rows over a rectangular area of approximately 1101.8 km^2 , giving 220,896 cells.

The vertical grid was adjusted as a deformed model to ensure the horizontal continuity over the modeled area. The simulation of groundwater flow was carried out for the two unconfined aquifers (Neogene and Paleogene aquifers) in a steady-state mode over a period of 10 years (3652 days). The groundwater budget of the catchment area was also evaluated in this study.

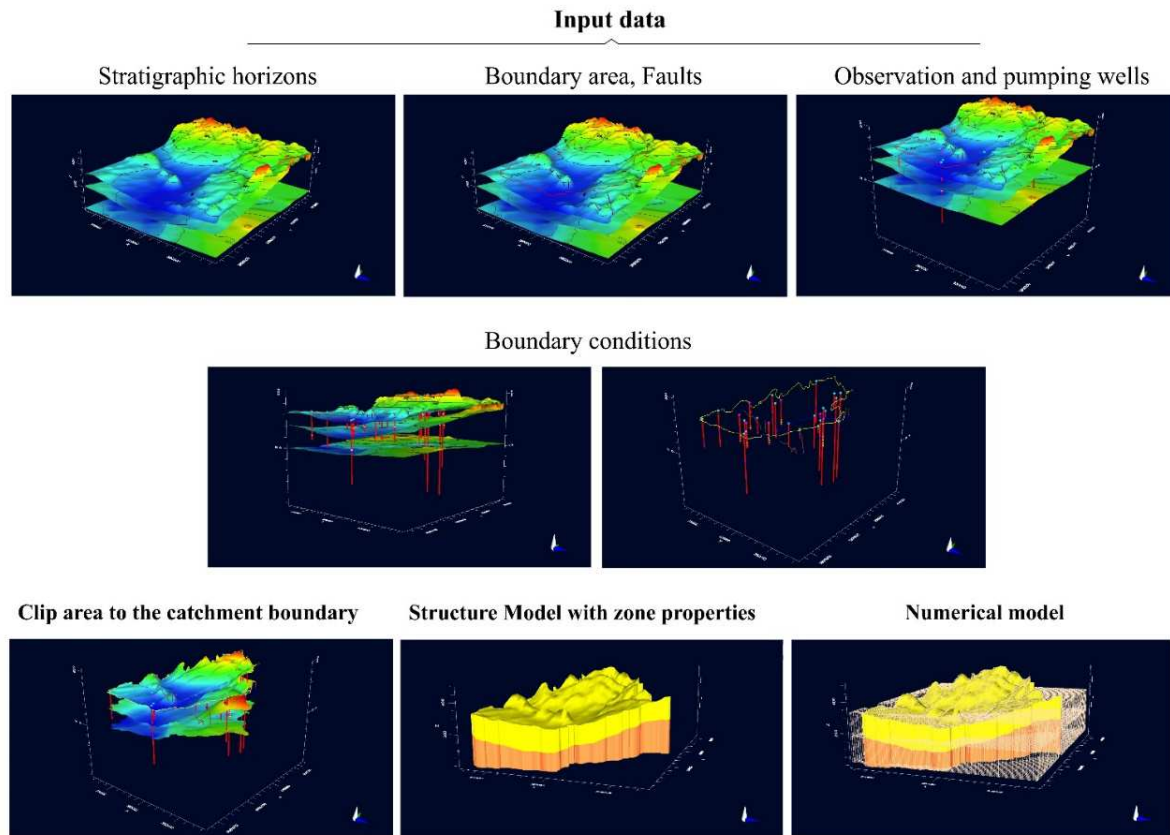


Fig. 8: General overview of the conceptual model of the catchment area

2.8 Boundary conditions

The groundwater boundary conditions of the catchment area were determined based on both the natural groundwater divides and the regional groundwater-contouring map. In this study, the groundwater flow system was determined by the following physical boundaries: constant heads (CHDs), no-flow boundaries, river (Al Qweek River), the potential groundwater recharge (R), the potential evapotranspiration (PET), and the wall boundary condition (Al Bredeh fault) (Fig. 9).

As mentioned above, the groundwater equipotential lines of both aquifers are relatively similar, with a general flow direction from the east and northeast to the southwestern site of the catchment (Fig. 4). Since many observation wells are located close to the boundary of the catchment area, the static hydraulic head in those wells was assumed as a constant head for each aquifer (R31, R36, H27, R140, R144, R146, R136, R124, and HC9).

The groundwater contour lines of the 1:200,000 Gruzgiprovodkhoz (1979) hydrogeological map were assumed as the initial groundwater heads of the region (Fig. 10). The hydraulic properties, bed soil texture, and flow canal geometric data of the Al Qweek River were obtained from different published and unpublished reports (BGR and MOI 2004; Sato 2010). Table 4 shows the main characteristics of Al Qweek River at the inlet and outlet points.

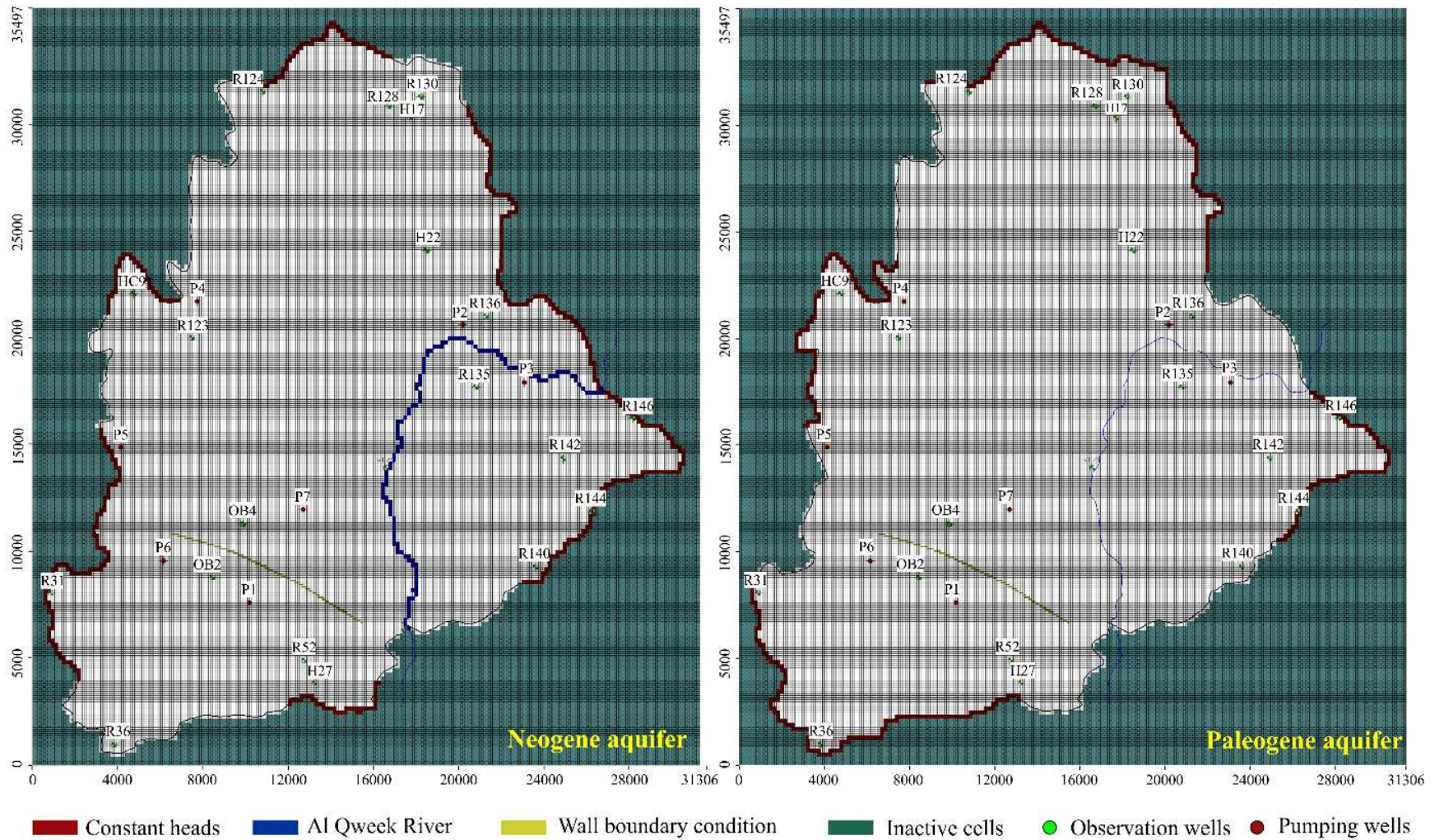


Fig. 9: The main boundary conditions of the catchment area

Tab. 4: The physical and hydraulic properties of Al Qweek River within the catchment area

Reaches	Avg. river stage (m)	Avg. riverbed bottom (m)	Avg. riverbed thickness (m)	K_z (m/day)	River width (m)	Riverbed soil texture		
						Sand %	Clay %	Silt %
Start	338	337	0.80	0.029	11.5	24	25	51
End	258	257	1.00	0.013	6.8	15	25	60

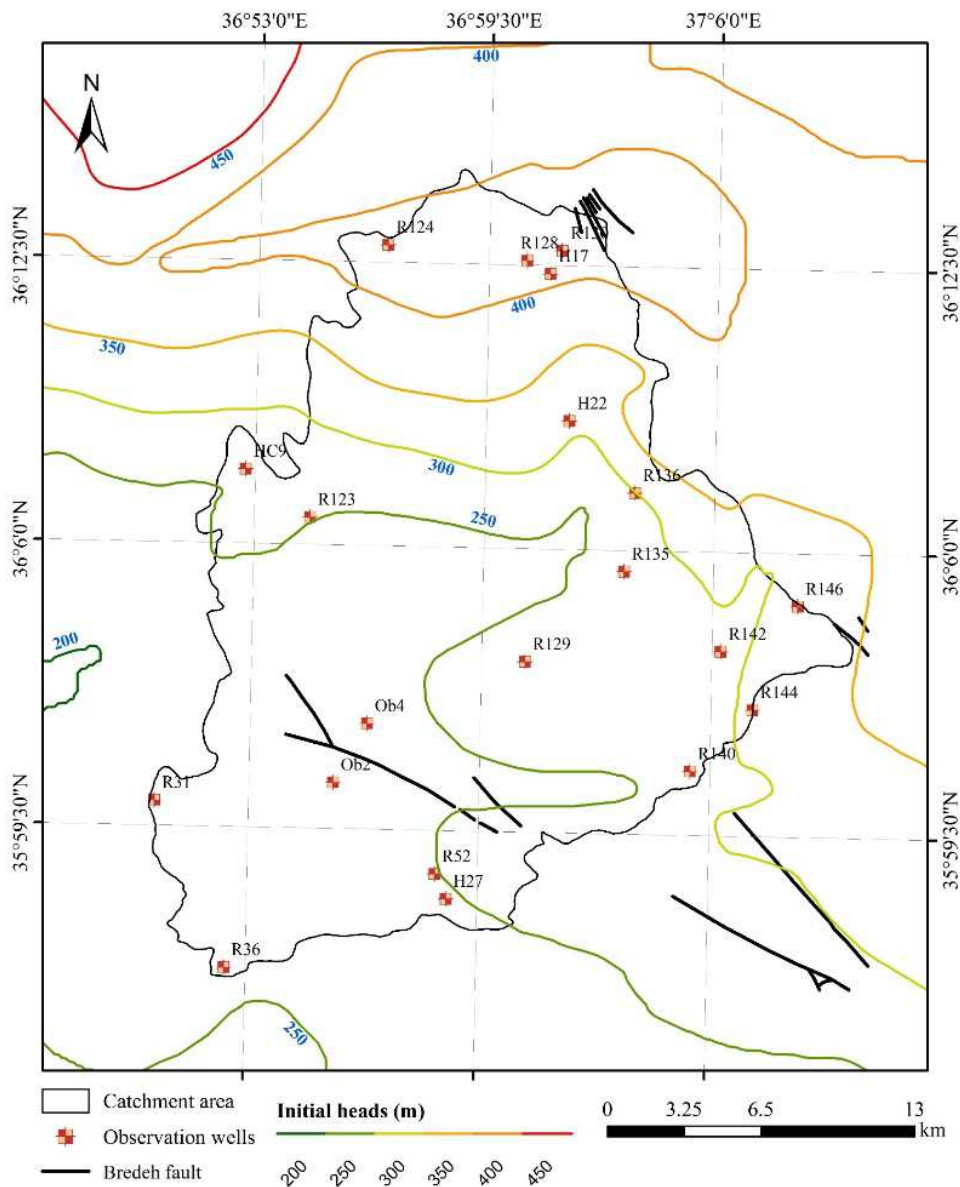


Fig. 10: Groundwater initial heads modified after Gruzgiprovdkhoz (1979)

According to the laboratory tests of the rock samples, the average porosity ranges from 0.50 in the Helvetian rocks (56 rock samples) to 0.46 in the Paleogene samples (32 records) (Gruzgiprovdkhoz 1982). The effective porosity of both aquifers was assumed to be greater than or equal to the specific yield, considering a small specific retention value for limestone formations of 2 % (Heath 1983). The hydraulic parameters of both aquifers are shown in Table 5. Groundwater in the region is mostly de-

rived from the second aquifer as a major source of fresh drinking water and for irrigation. The average pumping rate in the area ranges from about 32 m³/d to more than 1900 m³/d. Unfortunately, there are no continuous records of well abstraction in the region.

Tab. 5: The hydraulic properties of the Neogene and Paleogene aquifers in the region based on the data reported by Gruzgiprovodkhoz (1982)

<i>Aquifers</i>		<i>Neogene (Helvetian)</i>	<i>Paleogene (Eocene)</i>
Aquifer thickness (m)	Min.	23	10
	Max.	187	125
	Avg.	92	67
Well yield (L/s)	Min.	1.4	1
	Max.	14.1	13.6
	Avg.	5.6	4.9
Specific yield (S _y)	Min.	0.04	0.02
	Max.	0.5	0.5
	Avg.	0.3	0.3
Hydraulic conductivity (m/d)	Min.	0.05	0.01
	Max.	11	18.9
	Avg.	1.8	2.7
Rock porosity (%)	Min.	43	42
	Max.	59	51
	Avg.	51	46
Effective porosity	Avg.	0.2	0.2

2.9 Model calibration and sensitivity analysis

The calibration of groundwater model was carried out in two main stages: the *trial and error* method and the *automated parameter estimation* method using the PEST program (Doherty et al. 1994). The *trial and error* method was used to optimize the computed pressure heads and to correlate them with actual observed heads in 20 observation wells by adjusting the values aquifer hydraulic parameters and groundwater recharge. The target was to reach a normalized root mean squared error (*NRMSE*) of less than 5 % and standard error (*SE*) of estimation below 1 m, which is generally agreed for steady state flow and balance models (Barnett et al. 2012). The standard root mean squared error in percent represents the root mean squared error (*RMSE*) divided by the measured head ΔH as expressed by Eq. 6:

$$NRMSE = \frac{100}{\Delta H} \sqrt{\frac{1}{n} \sum_{i=1}^n (h_{ob,i} - h_{mod,i})^2} \quad (6)$$

where $h_{ob,i}$ represents the measured head h_i , while $h_{mod,i}$ is the calculated head at the same location n and time i .

The results of calibration, statistical parameters [residuals, standard error (m), normalized root-mean-square error, *NRMSE*, and the correlation coefficient], and zone budget were stored after each simulation for interpretation.

Once the model had reached its best convergence between observed and modeled heads, an automated parameter optimization was applied by means of PEST integrated into the visual MODFLOW (WinPEST). The hydraulic conductivity (K_x , K_y), specific yield, and groundwater recharge were used

in the optimization. The groundwater heads were used as the model objective function (ϕ) representing the sum of weighted squared deviations between the computed and observed heads. Thus, the lower the objective function, the better the correlation that can be achieved (Hill and Tiedeman 2006). Finally, the sensitivity analysis was applied to investigate the changes of the groundwater system with respect to the hydraulic conductivity, storativity, and groundwater recharge.

3 Results and discussion

3.1 Lithology and stratigraphic models

The lithological model of the study area is shown in Fig. 11. The results indicate significant thickness of the Upper Cretaceous deposits (dolomitized limestone) at average depths of 400 m below the ground surface. They constitute approximately 46 % of the model's total volume ($4.895 \cdot 10^{11} \text{ m}^3$). However, high-uncertainty is expected due to the limited number of boreholes that completely penetrate the Cretaceous formation in the region. In contrast, the Helvetian and Eocene formations constitute about 21 and 18 % of the lithological model, respectively. The calculated volumes of different lithological types are presented in Table 6. The results also revealed conformity between the Neogene and Paleogene deposits within the catchment area, while the Helvetian and Miocene basalt flow unconformably overlies the Neogene deposits in the eastern site of the area.

The marl and marly limestone of the Maastrichtian deposits spread in the region as impermeable layers and locally alternate with dolomitized limestones. These successions may be associated with a parasequence cycle (periodic) during the Late Cretaceous in the region, which is mainly affected by sediment flux that matches the water level rise of the Tethys Sea close to the coastal zone (Emery and Myers 1996). Moreover, the visual interpretation of the lithological sections of the region show a sequence of folds, subsurface joints and faults, which are invisible at the surface in the northern parts of the study area (Jebel Simon and Aleppo uplift). The surface distribution of the main outcropped formations is consistent with those on the geological map.

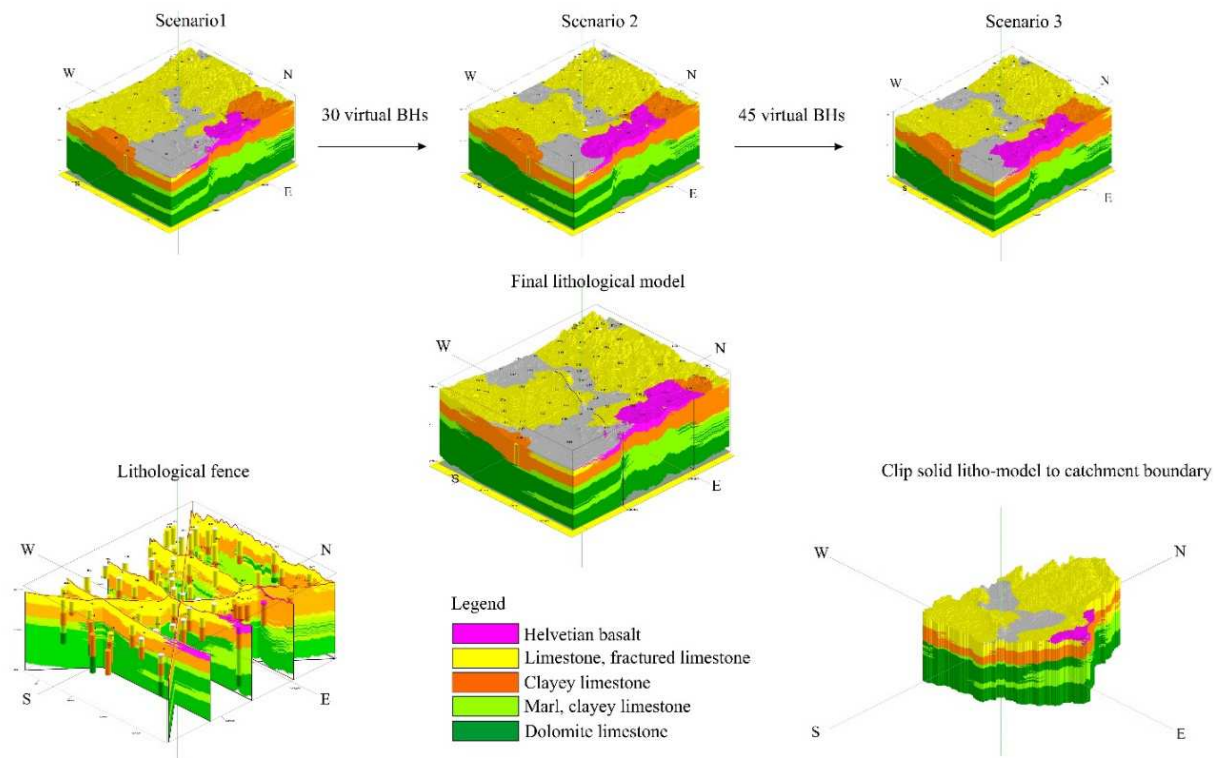


Fig. 11: The 3-D lithological model of the study area

Tab. 6: Volumetric calculation of the various lithological types in the model

<i>Litho-types</i>	<i>Basalt</i>	<i>Quaternary Sediments</i>	<i>Limestone</i>	<i>Clayey limestone</i>	<i>Marly limestone</i>	<i>Dolomitized limestone</i>	<i>Total</i>
Total volume (m ³)	1.08·10 ⁹	1.47·10 ⁹	1.02·10 ¹¹	8.99·10 ¹⁰	6.76·10 ¹⁰	2.27·10 ¹¹	4.90·10 ¹¹
Percentage (%)	0.22	0.32	20.90	18.35	13.81	46.40	100

On the other hand, the constructed stratigraphical solid model shows considerable thickness of the Helvetian limestone deposits in the study area, covering with consistent distribution the Paleogene deposits, as shown in Fig. 12. The interbedded layers are relatively flat with gentle slopes following the changes in the topographic surface. The volumetric calculations of different stratigraphical units show a significant thickness of the Miocene deposits within the study area with a total volume of $8.56 \cdot 10^{10} \text{ m}^3$, while the thickness of the Paleogene (upper and middle Eocene) deposits is about $9.34 \cdot 10^{10} \text{ m}^3$. The total volume of both strata forms 36.6 % of the model's total volume.

3.2 Relationship between resistivity and aquifer permeability

The three-dimensional resistivity model of the catchment area is depicted in Fig. 13. The model revealed obvious variation normal resistivity from 15 to 300 Ωm . Low resistivities were found in the impermeable formations of the marl, marly limestones, clay, and red clayey limestones of the outcropped Paleogene along the Al Qweek River in the north (Boreholes H22, H17). This can be explained by ion exchange in the layers with high content of clay minerals, which can lead to the increase of the electrical conductivity of the water and hosting formation (Keys and MacCary 1971). In contrast, moderate to high resistivities were found in the southwestern parts of the catchment area vary from 120 to 220 Ωm in the water-saturated/unsaturated horizons of the Helvetian. The maximum variation in the resistivity values was observed in the eastern parts of the Helvetian and Miocene basalt (Al Hass Mountain). The average resistivity values in this region can reach up to 300 Ωm . Hydrogeologically, the moderate resistivity values in the range of aquifers indicate potentially low to moderate mineralization, freshwater-yielding aquifers, and good groundwater quality (Hudson 1996).

Conversely, the high conductivity value (low resistivity) in the shallow horizons of the central and northeastern parts of the catchment may indicate poor-quality water and a potential contamination by the highly mineralized surface water of the Al Qweek River and distributed irrigation canals in the area or a type of mixing with high mineralized groundwater of deeper aquifers (Upper Cretaceous). Furthermore, the resistivity model suggests the eastern parts of the catchment area as potential recharge area (Helvetian outcrops and basalt flow).

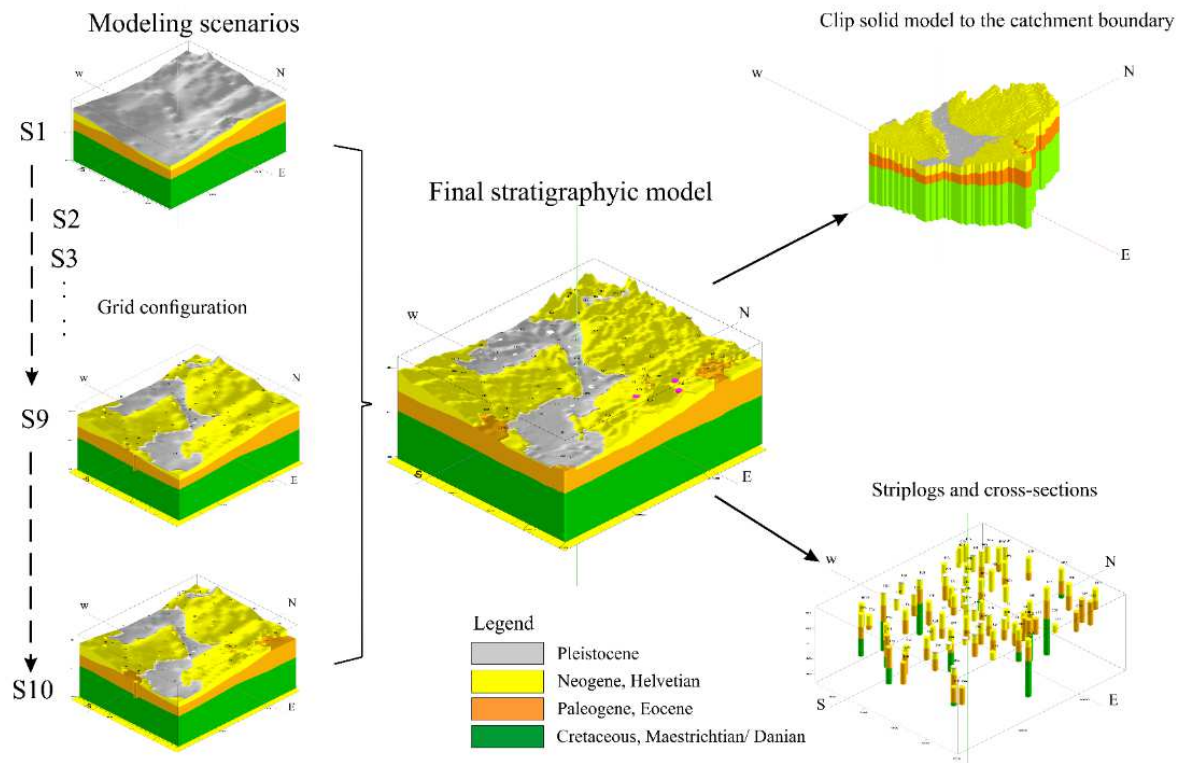


Fig. 12: The development of the 3-D stratigraphic model of the study area using advanced stratigraphic modeling in RockWorks

From the statistical point of view, a positive relationship was found between the aquifer hydraulic conductivity and average resistivity of the Neogene and Paleogene aquifers. For the Neogene aquifer, the results fit the squared-X model with an R^2 of 96.96% and a P-value of 0.0001. In contrast, an exponential relationship was found between the variables of the Paleogene aquifer with an R^2 of 98.95% and P-value of 0.0005 (Fig. 14). The equations of the fitted models for the Neogene Paleogene aquifers in the region can be expressed as follows:

$$K_N = -0.7039 + 0.000224(R)^2 \quad (7)$$

$$K_{Pg} = e^{(-2.929+0.03639(R))} \quad (8)$$

where K_N and K_{Pg} are the hydraulic conductivity (m/day) of the Neogene and Paleogene aquifers, respectively. R is the average resistivity in ohm meters

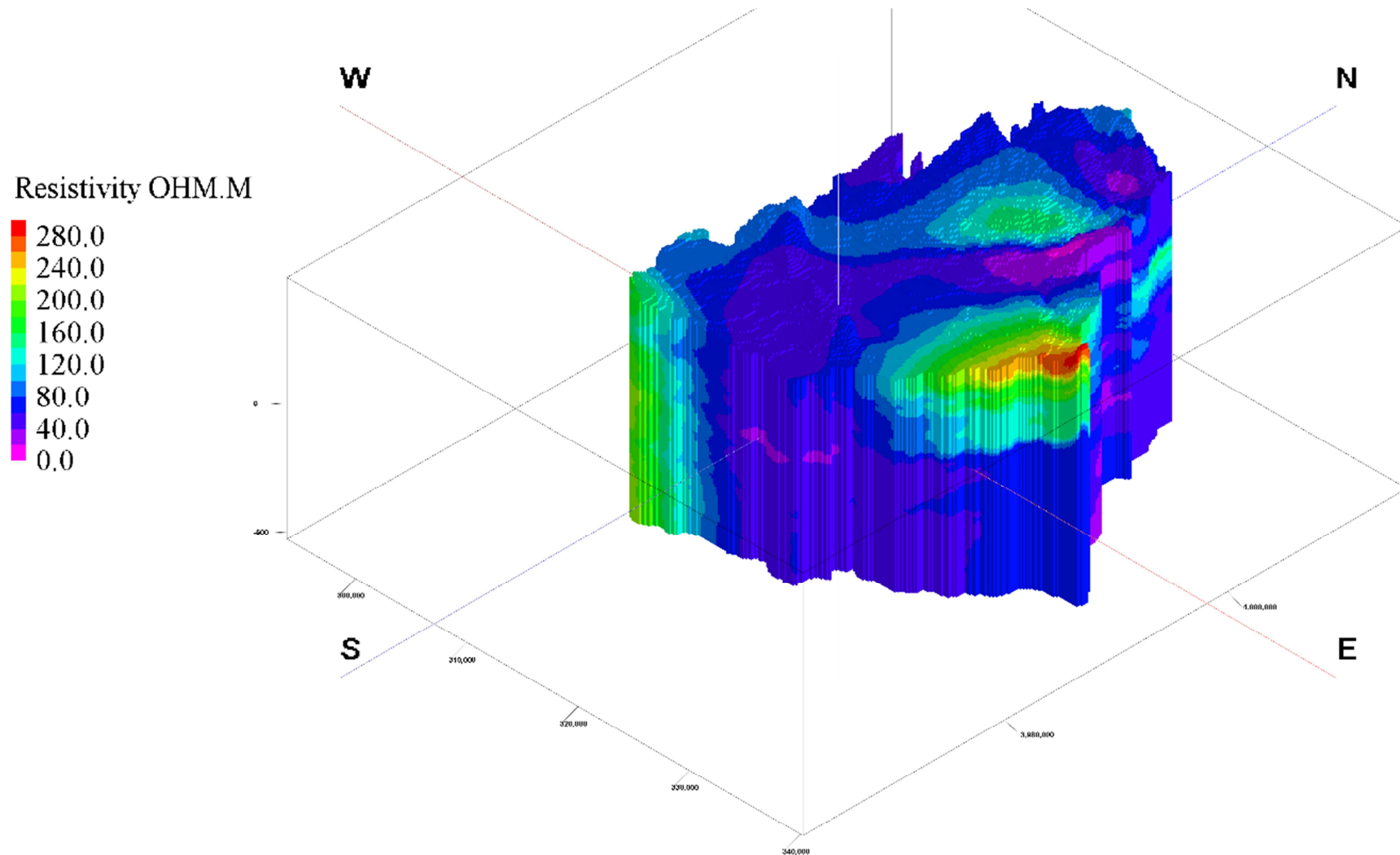


Fig. 13: Three-dimensional resistivity model of the catchment area

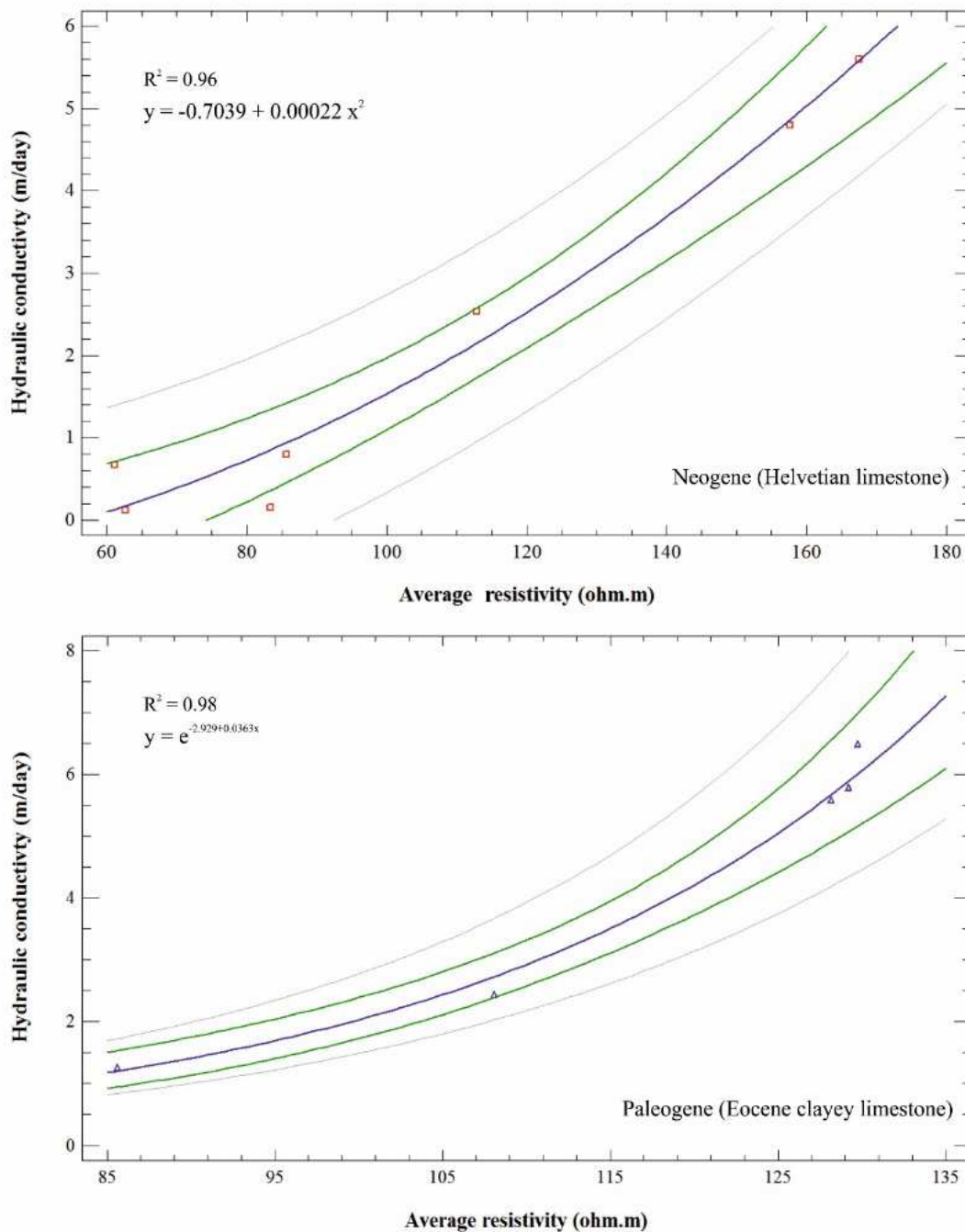


Fig. 14: Regression analysis describing the relationship between the aquifer permeability and average normal resistivity in the study area

3.3 Groundwater flow and budget

The simulation of the steady-state groundwater heads exhibited a general groundwater flow direction from the north and northeast (Jebel Simon and Aleppo uplift) to the southern parts of the catchment area (Tel Hadya) for the upper aquifer of the Helvetian limestone, with average decrease in the equipotential heads of about 140 m. The simulated head follow the gradient from the east (Al Hass Mountain) to the western parts of the region (Idlib Valley) for the second aquifer (Eocene clayey limestone) as depicted in Fig. 15.

The average difference in groundwater head in the second aquifer is relatively less severe than in the upper aquifer, with an average gradient of 20 m. Nevertheless, the second aquifer is significantly affected by groundwater abstraction in comparison to the upper aquifer. The average calculated draw-down in groundwater tables of the Paleogene aquifer ranges from 3 to 4 m in the region of Al Zerba and from 7 to 8 m in the Tel Hadya, while it ranges from 0.5 to 0.8 m in the Helvetian aquifer.

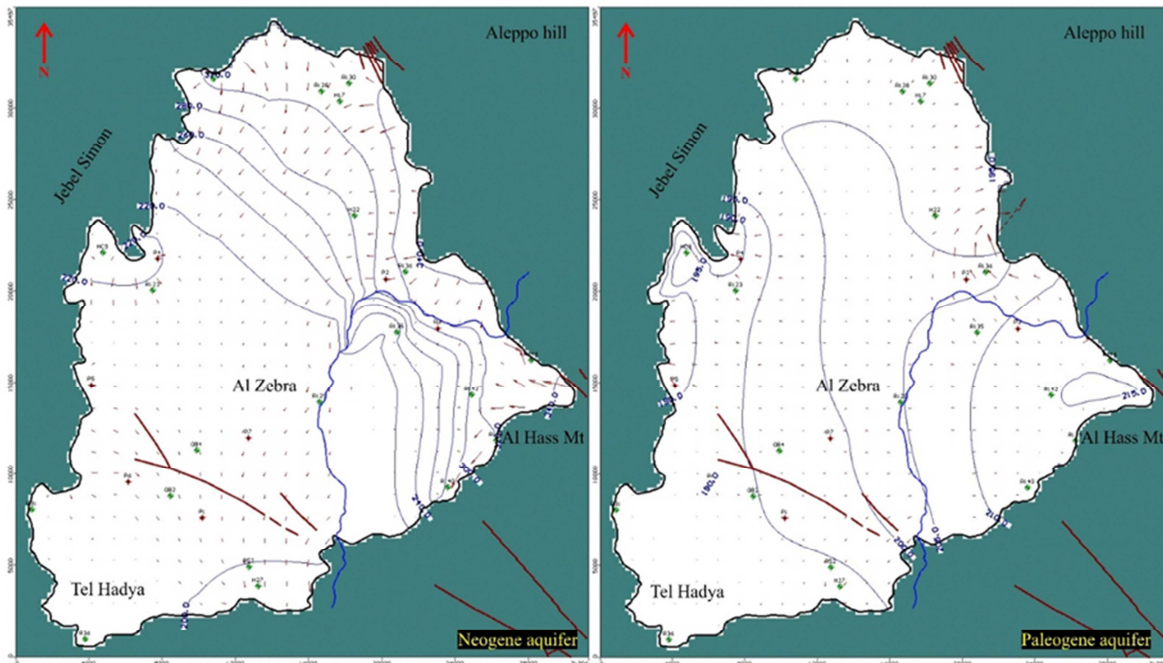


Fig. 15: Groundwater flow model of Al Zerba catchment

The visual interpretation of groundwater equipotential lines along Al Qweek River in the eastern parts of the catchment indicates a losing stream condition recharges the upper unconfined aquifer in form of focused groundwater recharge (Winter and Judson 1998). Furthermore, the simulation revealed that the outcropped formations of the Helvetian limestones in the north and eastern parts of the catchment act as recharge areas for the upper aquifer, with an average annual groundwater recharge of 30 mm/a.

This result indicates that the fractured zone of Al Bredeh has no significant impact on the groundwater flow direction, except for slight changes in the western parts, where groundwater tends to flow horizontally parallel to the strike direction in the upper aquifer.

Conversely, obvious horizontal shifts in the groundwater contour were found in the second aquifer around the Al Bredeh fault range from 100 to 250 m. The neighboring areas of the Al Hass Mountain to the east (the location of R146, R142, and R144) and the fractured zone could be considered as potential sources of groundwater interflow from the upper aquifer into the second aquifer of the Middle and Upper Eocene.

The final calibrated model represents a water budget discrepancy of <math><0.004\%</math> and a total inflow of 88046 m³/d in the upper zone (Helvetian aquifer), with a simulated river leakage of 3466.3 m³/d. Moreover, the total outflow into the second zone was estimated as 66236 m³/d. The total groundwater recharge in the region was estimated as 14228 m³/d (about 9.1 mm/a).

The model also shows a total contribution of the second aquifer to the total flow of 126. m³/d. The calculated groundwater abstraction of 5228 m³/d is mainly pumped from the second aquifer. Table 7 lists the results of the water budget of the Al Zebra catchment.

Tab. 7: The groundwater budget of the Neogene and Paleogene aquifers

		<i>Budget zones (m³/d)</i>	
		Neogene	Paleogene
Constant heads	In	70226	170.42
	Out	21343	61052
Recharge	In	14228	0.00
	Out	0.00	0.00
River	In	3466.3	0.00
	Out	422.33	0.00
Wells	In	0.00	0.00
	Out	0.00	5227.9
Inflow/outflow	Zone 1 to 2	66236	66236
	Zone 2 to 1	126.04	126.04
Total	In	88046	66406
	Out	88046	66406

3.4 Model calibration and sensitivity analysis

As mentioned above, the calibration of the groundwater flow model was carried out using 20 observation wells distributed within the catchment area. The *trial and error* calibration method showed that the model is primarily sensitive to the values of the hydraulic conductivity and groundwater recharge. The non-convergence between observed and calculated heads results in the areas with very low hydraulic conductivities close to the model boundary (< 0.005 m/d), or in high groundwater recharge over the southern bank of the Al Qweek river (observation well R135).

Table 8 lists the results of manual and automatic calibration. A correlation coefficient (R) of 0.994, a normalized root mean squared error of 5.14 %, and a standard error of 1.33 m were the best results achieved using the *trial and error* method. In contrast, the *automatic parameter optimization* using the PEST package improved the results by decreasing the $NRMSE$ to 3.39 % and the standard error to 0.85 m with a correlation coefficient between the observed and calculated heads of 0.998. Based on these results, the model is assumed reasonable and able to simulate the groundwater flow in the catchment area (Fig. 16).

On the other hand, the sensitivity test shows that the model is sensitive to the horizontal hydraulic conductivity (K_{x_4} , K_{x_5} , and K_{x_8}) in the adjoining areas of the Al Qweek River, Al Jamra Village to the east (R135 observation well), and in the fractured region (Al Bredeh zone). The relative sensitivities ranging from 2.06 to 2.63 as listed in Table 9. The results also indicate that the model is less sensitive to changes in the specific yield (S_y) (the relative sensitivity is ≤ 0.00). In contrast, groundwater recharge has a significant impact on the results, with an average relative sensitivity ranging from 0.018 to 1.04.

The calibrated model showed heterogeneous distribution of the horizontal hydraulic conductivities K_x and K_y vary from 2.9 to 3.1 m/d for the upper aquifer in the northern parts of the catchment (Jebel Simon), from 15 to 6.5 m/d in the south (Tel Hadya and Al Zerba region), and from 0.45 to 3.1 m/d in the east. In contrast, the hydraulic conductivities of the second aquifer decrease gradually from the northeastern to the southwestern parts of the catchment and vary considerably from 0.6 to 15 m/d. After calibration, the average simulated groundwater recharge in the catchment is 7 mm/a for the central region, while higher recharge rates were estimated in the adjacent area of Jebel Simon in the north and the western edges of Al Hass Mountain to the east. A relatively low groundwater recharge of < 5 mm/a was simulated over the Tel Hadya region.

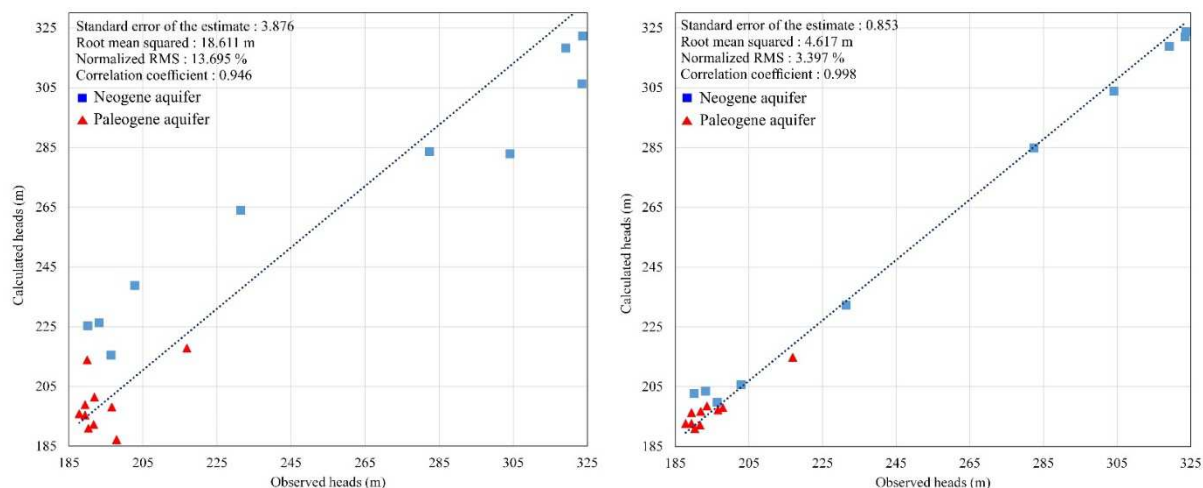


Fig. 16: Calculated versus observed groundwater heads of the Neogene and Paleogene aquifers

Tab. 8: Results of manual and automatic calibration of the steady-state groundwater flow model in the Neogene and Paleogene aquifers. The Min.Res. and Max.Res in the table represent the minimum and maximum residual in simulated groundwater heads

Run number	Min. Res. (m)	Max. Res. (m)	Mean. Res. (m)	SE (m)	RMSE (m)	NRMSE %	R
1	0.53	35.93	8.28	3.771	18.407	13.545	0.949
2	0.5	34.98	7.27	3.33	16.25	11.963	0.962
3	0.245	31.766	6.452	3.05	14.805	10.894	0.968
4	0.007	28.995	7.598	2.321	12.652	9.31	0.981
5	0.043	27.64	7.482	2.212	12.206	8.981	0.983
6	-0.244	25.631	6.891	2.015	11.164	8.215	0.986
7	0.668	19.073	4.893	1.717	8.941	6.579	0.991
8	-0.12	18.459	3.795	1.643	8.103	5.963	0.991
9	0.007	18.22	4.211	1.453	7.606	5.597	0.993
10	0.006	17.339	3.847	1.338	6.985	5.14	0.994
Automatic calibration with PEST							
Optimized parameters	Min. Res. (m)	Max. Res. (m)	Mean Res. (m)	SE (m)	RMSE (m)	NRMSE %	R
Kx, Ky, Sy	0.045	13.566	2.447	1.003	5.011	3.687	0.997
GWR/ R135	-0.04	13.67	2.725	0.967	5.019	3.693	0.997
GWR/R135, OB1, OB2	0.071	12.562	2.734	0.853	4.617	3.397	0.998

Tab. 9: Sensitivity analysis for the steady-state flow condition by means of changes in hydraulic conductivity and groundwater recharge

Parameter	<i>Iteration 1</i>		<i>Iteration 2</i>		<i>Iteration 3</i>		<i>Iteration 4</i>	
	Initial value	R. sensitivity	Value	R. sensitivity	Value	R. sensitivity	Value	R. sensitivity
Kx_1	3.1	0.726	2.700	0.678	2.919	0.719	2.919	0.719
Ky_1	3.1	0.000	3.100	0.000	3.100	0.000	3.100	0.000
Kx_2	4.5	0.133	4.537	0.185	5.112	0.224	5.112	0.224
Ky_2	4.5	0.000	4.500	0.000	4.500	0.000	4.500	0.000
Kx_3	1.5	0.249	1.881	0.317	1.657	0.309	1.657	0.309
Ky_3	1.5	0.000	1.500	0.000	1.500	0.000	1.500	0.000
Kx_4	0.01	2.062	0.020	2.462	0.024	2.634	0.024	2.634
Ky_4	0.01	0.000	0.010	0.000	0.010	0.000	0.010	0.000
Kx_5	0.05	0.844	0.033	1.275	0.027	1.500	0.027	1.500
Ky_5	0.05	0.000	0.050	0.000	0.050	0.000	0.050	0.000
Kx_6	5.4	0.534	15.000	0.480	15.000	0.484	15.000	0.484
Ky_6	5.4	0.000	5.400	0.000	5.400	0.000	5.400	0.000
Kx_7	0.45	0.390	0.328	0.599	0.216	0.864	0.216	0.864
Ky_7	0.45	0.000	0.450	0.000	0.450	0.000	0.450	0.000
Kx_8	6.5	0.844	15.000	1.078	15.000	1.008	15.000	1.008
Ky_8	6.5	0.000	6.500	0.000	6.500	0.000	6.500	0.000
R1	20	1.039	1.000	0.161	1.000	0.294	7.000	0.148
R2	35	0.038	40.000	0.049	40.000	0.159	35.000	0.036
R3	45	0.823	27.726	0.630	1.000	0.449	30.000	0.579
R4	45	1.032	40.000	0.844	1.000	0.018	5.000	0.08

4 Conclusions

Three-dimensional stratigraphic and lithological models provide valuable information about the distribution of different lithofacies and formations between the boreholes, enabling a better understanding of the hydrostratigraphical successions and the model complexity. The lithological model offered a more reasonable representation of the geology and outcropped rocks, sedimentation conditions, sub-surface faults, and groundwater system in the 3-D space.

On the other hand, geophysical data of boreholes deliver important information about the spatial distribution of the aquifer systems. Furthermore, they offer the possibility of calculating the hydraulic parameters of hydrogeological successions in the absence of field hydraulic measurements, particularly in deep aquifers, where pumping tests are usually expensive and require special equipment.

This study suggests a hydraulic connection between Al Qweek River and the upper aquifer of the Helvetian. It also indicates an indirect impact of the fractured zone on the groundwater flow direction in shallow horizons. The region is characterized by relatively low recharge values.

The study also showed that sensitivity analysis is an essential tool for investigating the various critical conditions and stresses within hydrogeological units, promoting the calibration results by ensuring the field observations. The groundwater flow model of the study area was relatively sensitive to changes in hydraulic conductivity and groundwater recharge and less sensitive to the aquifers' specific yield.

5 Acknowledgments

The authors thank Dr. Adriana Bruggeman, Dr. Elco Luijendijk, and Dipl.-Geol. Fabian Helms from the Federal Institute for Geosciences and Natural Resources (BGR) for their support and provision of data. Thanks are due to the Syrian Ministry of Irrigation and Water Resource Sector of Aleppo. Special thanks are also due to the staff of RockWare, Jim Reed and Tom Bresnahan, for their technical support.

6 List of references

- Abo RK, Merkel BJ (2015) Comparative estimation of the potential groundwater recharge in Al Zerba catchment of Aleppo basin, Syria. *Arabian Journal of Geosciences* 8 (3):1339-1360. doi:10.1007/s12517-013-1222-9
- Alkhalifah T, Rampton D (2001) Seismic anisotropy in Trinidad: A new tool for lithology prediction. *The Leading Edge* 20 (4):420-424
- Anderson MP, Woessner WW (1992) *Applied groundwater modeling: simulation of flow and advective transport*, vol 4. Gulf Professional Publishing,
- Bachrach R, Perdomo J, Mallick S, Dutta N Propagating seismic data quality into rock physics analysis and reservoir property estimation: case study of lithology prediction using full waveform inversion in clastic basins. In: 2003 SEG Annual Meeting, 2003. Society of Exploration Geophysicists,
- Barnett B, Townley L, Post V, Evans R, Hunt R, Peeters L, Richardson S, Werner A, Knapton A, Boronkay A (2012) *Australian groundwater modelling guidelines*. National Water Commission, Canberra
- Bartier PM, Keller CP (1996) Multivariate interpolation to incorporate thematic surface data using inverse distance weighting (IDW). *Computers & Geosciences* 22 (7):795-799. doi:http://dx.doi.org/10.1016/0098-3004(96)00021-0
- Bell FG (2007) *Engineering Geology* Butterworth-Heinemann, UK
- Berg R, Russell H, Thorleifson H Introduction- Three-Dimensional Geological Mapping: An international Perspective In: *Three-Dimensional Geological Mapping, Workshop Extended Abstracts*, Geological Society of America, Portland, Oregon 2009. vol 2009-4. ISGS open File pp 3-74
- BGR, MOI (2004) *Initial assessment study of water sector management in the Syrian Arab Republic*. Federal Institute for Geosciences and Natural Resources & Syrian Ministry of Irrigation, Damascus, Syria
- Busch J, Fortney W, Berry L (1987) Determination of lithology from well logs by statistical analysis. *SPE Formation Evaluation* 2 (04):412-418
- Chaimov TA, Barazangi M, Al-Saad D, Sawaf T, Gebran A (1990) Crustal shortening in the Palmyride fold belt, Syria, and implications for movement along the Dead Sea fault system. *Tectonics* 9 (6):1369-1386
- Chiang W-H, Chiang W (2001) *3D-groundwater modeling with PMWIN*, vol 346. Springer,
- Davidson JP, Reed WE, Davis PM (1997) *Exploring earth: an introduction to physical geology*. Prentice Hall,
- Doherty J, Brebber L, Whyte P (1994) *PEST: Model-independent parameter estimation*. Watermark Computing, Corinda, Australia 122
- Doyen P, Guidish T, de Buyl M (1988) *Lithology Prediction from Seismic Data: A Monte Carlo Approach* s 8.6.
- Emery D, Myers K (1996) *Sequence stratigraphy*. London, Uxbridge:297
- ESRI Inc (2011) *ArcGIS Desktop: Release 10.1*. Environmental Systems Research Institute, CA
- Freeze R, Cherry J (1979) *Groundwater*. 1 edn. Pentice Hall, New Jersey
- Fung CC, Wong KW, Eren H (1997) Modular artificial neural network for prediction of petrophysical properties from well log data. *Instrumentation and Measurement, IEEE Transactions on* 46 (6):1295-1299
- GCHS (1999) *Hydrogeological Investigations of Aleppo Basin, Phase 1*. Homs, Syria
- Gruzgiprovodkhoz (1979) *Hydrogeological and hydrological surveys and investigation in four areas of Syrian arab republic, Aleppo area (Hydrogeological map scale 1:200,000)*. Gruzgiprovodkhoz, Tbilisi
- Gruzgiprovodkhoz (1982) *Hydrogeological and hydrological surveys and investigations in four areas of the Syrian Arab Republic*. Georgian State Institute for Design of Water Resources, Tbilisi, Georgia
- Harbaugh AW (2005) *MODFLOW-2005, the US Geological Survey modular ground-water model: The ground-water flow process*. US Department of the Interior, US Geological Survey Reston, VA, USA,
- Heath RC (1983) *Basic ground-water hydrology*, vol 2220. US Geological Survey,
- Hill MC, Tiedeman CR (2006) *Effective groundwater model calibration: with analysis of data, sensitivities, predictions, and uncertainty*. John Wiley & Sons,

- Hudson JD (1996) Use of geophysical logs to estimate the quality of ground water and the permeability of aquifers, Water-Resource Investigations Report. U.S. Geological Survey Albuquerque, New Mexico
- Hunt RJ, Feinstein DT (2012) MODFLOW-NWT: Robust Handling of Dry Cells Using a Newton Formulation of MODFLOW-2005. *Groundwater* 50 (5):659-663
- Hyndman DW, Day-Lewis FD, Singha K (2013) *Subsurface hydrology: data integration for properties and processes*, vol 171. John Wiley & Sons,
- ICARDA (2000) Syria: Geology and Derived Aquifer Location and Properties, Scale 1:1,500,000.- Annex to Research Report "An Overview of the Water Resources in Syria" prepared by R. Hoogeveen & E. De Pauw within the framework of the Natural Resource Management Program, sponsored by USAID-CGIAR Linkage Fund, GIS handling by A. Oberle, A. Balikian & B. Nseir. Aleppo, Syria
- IFAD (2010) Syrian Arab Republic: Thematic study on land reclamation through de-rocking. Near East and North Africa Division, Programme management department Rome, Italy
- Isaaks EH, Srivastava RM (1989) *Applied geostatistics*, vol 2. Oxford University Press New York,
- JICA (1997) The study on water resource development in the northwestern and central basin in the Syrian Arab Republic (phase 1). Sanyu Consultants Inc, Tokyo
- Keys WS, MacCary LM (1971) Application of borehole geophysics to water-resources investigations. US Government Printing Office,
- Luijendijk E (2003) Groundwater resources of the Aleppo basin, Syria. MSc Thesis, Vrije Universiteit Amsterdam, The Netherlands,
- Luijendijk E, Bruggeman A (2008) Groundwater resources in the Jabal Al Hass region, northwest Syria: an assessment of past use and future potential. *Hydrogeology Journal* 16 (3):511-530
- Martin (1999) Water availability and water use in Syria. Report for the World Bank, Washington, DC.
- McDonald MG, Harbaugh AW (1988) A modular three-dimensional finite-difference ground-water flow model. vol Book 6, Chap A1, Open file Report 83-875. U. S. Geological Survey Techniques of Water-Resource Investigation, Reston, Virginia, USA
- McDonald MG, Harbaugh AW, the original authors of M (2003) The History of MODFLOW. *Ground Water* 41 (2):280-283. doi:10.1111/j.1745-6584.2003.tb02591.x
- Mukherjee S, Jha V (2011) Role of Lithology and Rock Structure in Drainage Development in the Kaliani River Basin, Assam, India. *Ethiopian Journal of Environmental Studies and Management* 4 (2):61-68
- Ninomiya Y, Fu B, Cudahy TJ (2005) Detecting lithology with Advanced Spaceborne Thermal Emission and Reflection Radiometer (ASTER) multispectral thermal infrared "radiance-at-sensor" data. *Remote Sensing of Environment* 99 (1):127-139
- Niswonger RG, Panday S, Ibaraki M (2011) MODFLOW-NWT, a Newton formulation for MODFLOW-2005. *US Geological Survey Techniques and Methods* 6:A37
- Olvmo M, Johansson M (2002) The significance of rock structure, lithology and pre-glacial deep weathering for the shape of intermediate-scale glacial erosional landforms. *Earth Surface Processes and Landforms* 27 (3):251-268
- Peng S, Zhang J (2007) *Engineering geology for underground rocks*. Springer,
- Pinder GF, Celia MA (2006) *Subsurface hydrology*. John Wiley & Sons,
- Ponikarov (1964) Geological map of Syria, Aleppo area scale 1:200,000. Technoexport, Moscow
- Reed JJ (1962) The importance of lithology in determining response to metamorphism and tectonic forces. *New Zealand Journal of Geology and Geophysics* 5 (1):86-91. doi:10.1080/00288306.1962.10420111
- RockWare Inc (2010) *Rockworks 15 user's manual*.
- Rowan LC, Mars JC (2003) Lithologic mapping in the Mountain Pass, California area using advanced spaceborne thermal emission and reflection radiometer (ASTER) data. *Remote sensing of Environment* 84 (3):350-366
- Sato T (2010) Soil Salinity and Sodicity Levels in Wastewater Irrigated Soils in a Peri-Urban Area of Aleppo Region, Syria. In. *Sustainable management of saline waters and salt-affected soils for agriculture: Proceed-*

- ings of the Second Bridging Workshop Nov 2009, International Center for Agricultural Research in the Dry Areas (ICARDA), Aleppo, Syria pp 73-78
- Schlumberger (2009) Hydro GeoBuilder user's Manual.
- Schlumberger (2010) Visual MODFLOW 2011.1. Users Manual
- Selkhozpromexport (1979) Hydrogeological and hydrological survey and investigation in four areas of Syrian Arab Republic (vol 2). Tiflis, Georgia
- Stadler S, Geyh M, Ploethner D, Koeniger P (2012) The deep Cretaceous aquifer in the Aleppo and Steppe basins of Syria: assessment of the meteoric origin and geographic source of the groundwater. *Hydrogeology Journal* 20 (6):1007-1026
- Stone WJ (1999) *Hydrogeology in practice*. Other Information: PBD: 1999.
- Thompson GR, Turk J (1998) *Introduction to physical geology*. Saunders College Pub.,
- UN-ESCWA (1997) Report on mission to Syrian Arab Republic (during the period 10-20 Jun 1997). Hydrogeologic advice to ICARDA on sustainable agricultural groundwater management in dry areas. . W. Wagner, Beirut
- UNEP (1997) *World atlas of desertification*. Edward Arnold, London
- Wendlandt RF, Bhuyan K (1990) Estimation of Mineralogy and Lithology from Geochemical Log Measurements (1). *AAPG Bulletin* 74 (6):837-856
- Winter TC, Judson HW (1998) *Ground water and surface water a single resource*. U.S. Geological Survey Circular 1139. DIANE Publishing, Denver, Colorado
- Wolfart R (1966) *Zur Geologie und Hydrogeologie von Syrien: unter besonderer Berücksichtigung der süd-und nordwestlichen Landesteile [On the geology and hydrogeology of Syria, with special reference to the southern and northwestern regions of the country]*. Bundesanstalt f. Bodenforschung, Hanover, Germany
- Zanchi A, Battista Crosta G, Nasser Darkal A (2002) Paleostress analyses in NW Syria: constraints on the Cenozoic evolution of the northwestern margin of the Arabian plate. *Tectonophysics* 357 (1):255-278

Modeling groundwater flow in Aqra Plain unconfined aquifer, north of Iraq

Jassas, Hussein Department of Hydrogeology, Institute of Geology, Technische Universität Bergakademie Freiberg, Gustav-Zeuner-Str. 12, 09599 Freiberg, Germany; email: husseinjassas@yahoo.com
Iraqi Geological Survey, Baghdad, Iraq

Kanoua, Wael Department of Hydrogeology, Institute of Geology, Technische Universität Bergakademie Freiberg, Gustav-Zeuner-Str. 12, 09599 Freiberg, Germany; email: wael_kanoua@yahoo.com
Chemical and Petroleum Engineering Faculty, Al Baath University, Homs, Syria

Merkel, Broder Department of Hydrogeology, Institute of Geology, Technische Universität Bergakademie Freiberg, Gustav-Zeuner-Str. 12, 09599 Freiberg, Germany; email: merkel@geo.tu-freiberg.de

Abstract: Groundwater flow modeling with MODFLOW-2000 was used to determine the water budget for the Aqra Plain unconfined aquifer and to quantify the fluxes between groundwater and the river. The study area (1070 km²) is part of the Aqra Plain which represents the middle part of Alkhazir Gomal River Basin and is located in the north of Iraq. The explicit activities in this plain are rain-fed farming of wheat and barley and irrigated vegetables growing along the Al-Khazir River. In the last decade, however, was switched to sprinkler irrigation to some extent to compensate the shortage in rainfall. Irrigation depends mainly on groundwater extracted from the underlying unconfined aquifer which is considered the major source for domestic and agricultural uses in the Aqra Plain. Therefore, steady state simulation was applied using observed groundwater levels from 2011-2012 to calibrate the model and to investigate if the aquifer's utilization is sustainable. During the aforementioned time period the total water inflow was estimated to be $171 \times 10^6 \text{ m}^3$ (65% as losing streams and 35% as direct recharge) and the total discharge was estimated with $171 \times 10^6 \text{ m}^3$ (92% as baseflow and 8% as an extracted water). The results show that groundwater is currently under sustainable use and that the aquifer has a high capacity for further water extraction. Moreover, advective transport simulation was performed using particle tracking by MODPATH to investigate the migration of potential pollutants from recharge to discharge areas and their potential speed.

Keywords: Al-Khazir River, groundwater, MODFLOW, Aqra Plain Aquifer, water budget

1 Introduction

Most countries in the Middle East rely on groundwater to meet their water-supply needs (Mukherjee et al. 2002). The global demand for this resource has increased from 126 (± 32) km³ in 1960 to 283 (± 40) km³ in 2000 due to population growth, development in agricultural and industrial sectors, and climate change (Wada et al. 2010). Therefore, attention should be drawn to manage the limited groundwater resources to avoid over extraction of the aquifers.

Aqra plain in Iraq constitutes the central part of Al-Khazir Gomal Basin far north of Iraq. Groundwater represents the main source of freshwater in addition to Alkhazir River in the central sector of the plain. More than 30 % of the plain is cultivated by rain fed barley and wheat, while vegetable and raw crops are cultivated along Al-Khazir River. Groundwater was used in the past mainly for domestic purposes. However, in the last decade under scarcity of rainfall on the one side and agricultural development on the other side sprinkler irrigation utilization in farming with groundwater has increased significantly, which is evidenced by more than 250 governmental wells and an unknown number of private wells being drilled in the region in the last 10 years.

In comparison with previous studies (Al-Sam and Hanna 1981), one cannot grasp a significant difference in groundwater qualitatively and quantitatively, because there is no significant change in groundwater depth and groundwater chemistry. Nevertheless, if groundwater exploitation continues rising at the pace of the last decade there might be irreversible negative qualitative and quantitative effects on the groundwater in the coming decades. Although the region of interest was part of different studies (Parsons Company in (1950s), Krasny (1983), Stevanovic & Marković (2004) and Stevanovic & Iurkiewicz (2004), Stevanović et al. (2009), Al-Basrawi (2006) and Al-Jiburi (2007)), those studies were conducted on a regional scale and no detailed information are available about the region of interest. The only detailed hydrogeological and hydrochemical study about Alkhazir-Gomal Basin was conducted by Al-Sam and Hanna (1981), especially for the inter-granular aquifer in the middle part of the basin (second region). The researchers reported that the groundwater in Alkhazir-Gomal Basin is fresh (400 mg/l in average) and the predominant water type is Ca-HCO₃. Their pumping test in the second region revealed a high transmissivity (7753 m²/day) nearby Alkhazir river course, 2000 m²/day in the middle region, and >100 m²/day near the hydrogeological boundaries. This study concluded that the amount of water required for agricultural and domestic uses were two times less than the dynamic resource of the unconfined aquifer in the second region.

Unfortunately, these few available studies in the area of interest neither evaluated the sustainability of the utilization regarding the aforementioned aquifer under the existing stress conditions nor the potential migration of pollutants through the basin. Therefore, it is important to look into the subsurface and investigate groundwater flow processes with respect to the geological structure of the basin. The only way to accomplish this goal is groundwater flow and transport modeling, as it is an important tool to predict the response under particular conditions. Groundwater models provide additional insight into the complex system behavior and can assist in developing proper management strategies.

The study herein used Visual Modflow “MODFLOW-2000” (Harbaugh et al. 2000) and the advective transport package “MODPATH” (Pollock 1994) to build a steady state groundwater flow model to determine groundwater budgets, evaluate the interaction between the unconfined aquifer and the river, and to model and predict flow paths and to estimate groundwater travel time (mean residence times). The model was used as a management tool for assessing the current situation of the basin. This model is an attempt to give a comprehensive vision to improve the water resources planning and management and ensure the save and sustainable use of groundwater.

2 Study area

2.1. Geographical setting and climate

The Aqra Plain Aquifer system, shown in Figure 1, is the most important aquifer in entire Iraq regarding its quality and quantity (Al-Sam & Hanna 1981). It is bordered from the north and northwest by the Aqra Mountain series, from the south by the Bardarash and Maklub Mountains, and from the west by Sinjar Mountain. The plain covers an area of 1070 km² and represents the central part of Alkhazir Gomal Basin, overlaying a vast syncline extends between Aqra and Bardarash Mountains. The major part of the Aqra plain is located between an altitude of 321 and 563 masl. The plain drains towards Alkhazir Gomal River and then to Greater Zap River, which finally flows into the Tigris river. Alkhazir River and its tributary Gomal River cross the plain in addition to several intermittent watercourses. The plain is made up of Quaternary and Pliocene alluvial sediments, which consist mainly of gravel, sand, and silt interbedded with thin layer of clay and silty clay. Due to the similarity in lithology and groundwater head these two formations are considered as one hydrological unit.

The plain of Aqra has a semi-arid climate with hot and dry summers, and cold and wet winters. Annual rainfall obtained from Aqra meteorological station (latitude 36.71 and longitude 43.85) for the period (2001-2011) is about 650 mm, and mainly occurs in the wet season (October-April).

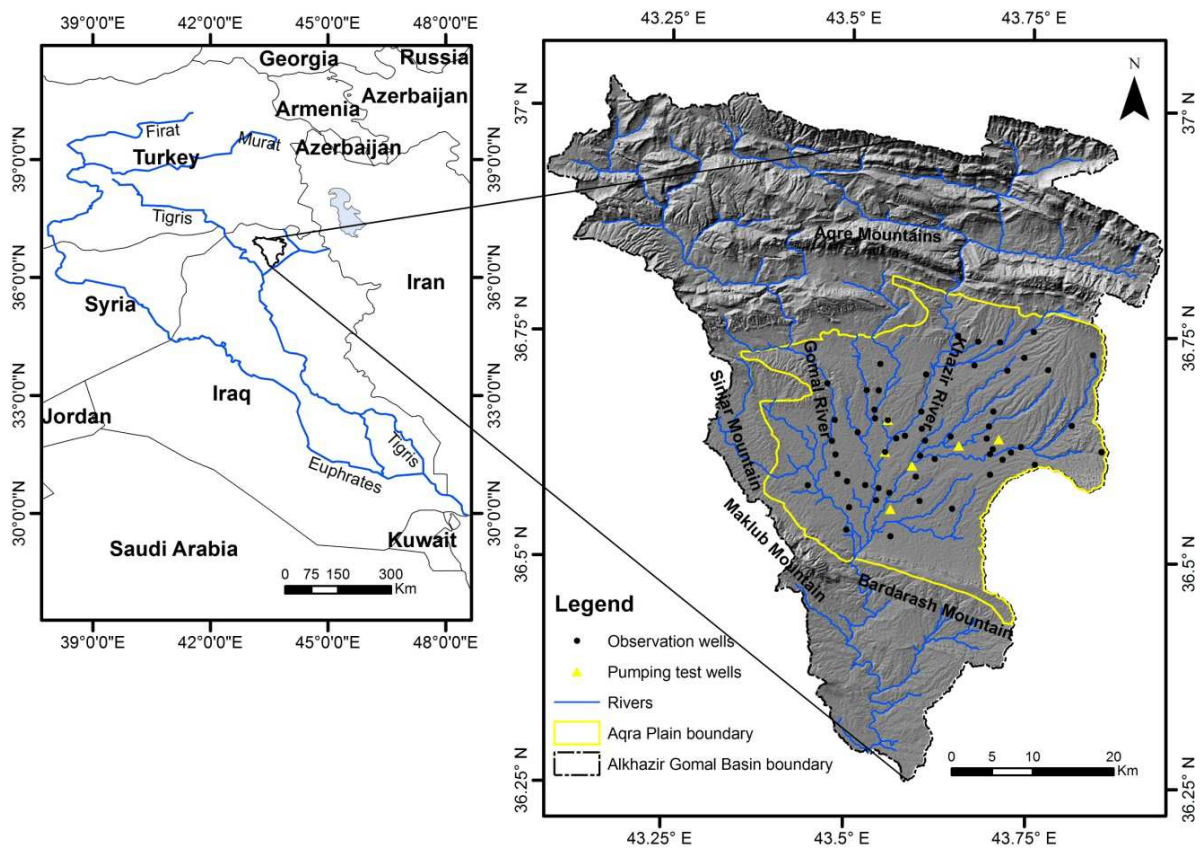


Fig. 1: Location map, boundary of Alkhazir Gomal Basin, boundary of modeled Aqra Plain Aquifer with the locations of observation and pumping test (modified after Jassas and Merkel 2015)

2.2. Hydrological setting

Alkhazir River and its tributary Gomal River originate from Aqra Mountains and drain about 3185 km² of mostly mountainous land. The Alkhazir is the major tributary to Greater Zap River, which is one of the main tributaries of Tigris River. The total length of the Alkhazir River is about 96 km, and the reach of the river within Aqra Plain is about 38 km. In dry seasons, the springs in the mountainous area and the mountain front deliver most of the of the river discharge. Furthermore, in dry season, Alkhazir river water infiltrates through high permeable alluvial deposits into the Aqre plain aquifer and disappears completely after passing about 15 km within Aqra Plain. Thereafter, groundwater in the aquifer flows downstream and discharges directly as baseflow in Alkhazir River course.

In wet season most of the small tributaries lose large part of their water in the high permeable alluvial deposits of the main valley before they join the Alkhazir river. Discharge records of Alkhazir river show that the annual streamflow during (2011-2012) is $363 \times 10^6 \text{ m}^3$ (Director General Of Irrigation 2012), about 52% of which occurs as baseflow discharge. The baseflow will be used later to validate groundwater model.

2.3. Geological and hydrogeological setting

The geological and hydrological description of the study area was summarized by Al-Sam & Hanna (1981), Sissakian & Galib (1995), and Jassim & Goff (2006). In general, Aqra Plain (Fig. 2) represents the central part of Alkhazir Gomal basin, underlain by Pliocene and quaternary sediments and surrounded by mountainous areas with rock outcrops ranging in age from Miocene to cretaceous. Aqra Plain is an unconfined aquifer composed of unconsolidated alluvial fills of Bia Hassan Formation (Pliocene), which consists mainly of gravel, sand, and silty clay. The thickness of these sediments, which are considered the main water bearing rocks, ranges between 38 and 250 m. The unconfined aquifer is underlain by 4 to 20 m impervious clay bed which extends over the whole entire aquifer and separates Bia Hassan Formation from the confined aquifer of Late Miocene Mukdadiyah Formation.

Most of Aqra plain is covered by alluvial Quaternary sediments ranging in thickness from 5 to 40 m, except limited Pliocene outcrops in the foothills. Due to the similarity in lithology between Quaternary and Pliocene sediments they are considered as one hydrogeological unit. An isopach map of this uppermost aquifer was drawn depending on the information derived from 57 lithology log boreholes spread over all the Aqra plain and penetrating the entire thickness of the aquifer. The maximum thickness observed is between Alkhazir and Gomal river (in the plain center), and it decreases towards the borders of the plain. As is the characteristic of the alluvial sediments, there is a significant lateral variation in lithology, and consequently variations in aquifer parameter (transmissivity, hydraulic conductivity, and specific yield).

The Bia Hassan formation outcrops and the high permeable Quaternary sediments of slope sediments and alluvial sediments along the rivers are considered the main recharge areas. Groundwater flows from the foothills and from plain margins towards the lower lands near the center of the plain, finally discharging into Alkhazir and Gomal rivers. Groundwater levels range from 322.5 at the outlet to 533.2 masl at northeast. The regional flow direction is from the north to the south, and locally flows from the north, the northern east, and northern west toward the main course of Alkhazir River. The average hydraulic gradient of about 6.3 m/km increases towards the foothills of Aqra Mountains in the north and northern east and decrease in the central parts. This is due to the topography and to the high transmissivity of the sediments in the central parts of the plain.

The results of pumping test conducted in 1981 by Al-Sam & Hanna (1981) shows that the transmissivity range from 110 to 7753 m²/day. Higher values (7753 m²/day) are found in the vicinity of the river in the center of the plain and lower towards the plain margins. The storativity coefficient varies between 2.1×10^{-4} - 1×10^{-1} . Rather low storativity values can be attributed to the presence of clay lenses in alternation with water bearing rocks; making the unconfined aquifer semi-confined in some places.

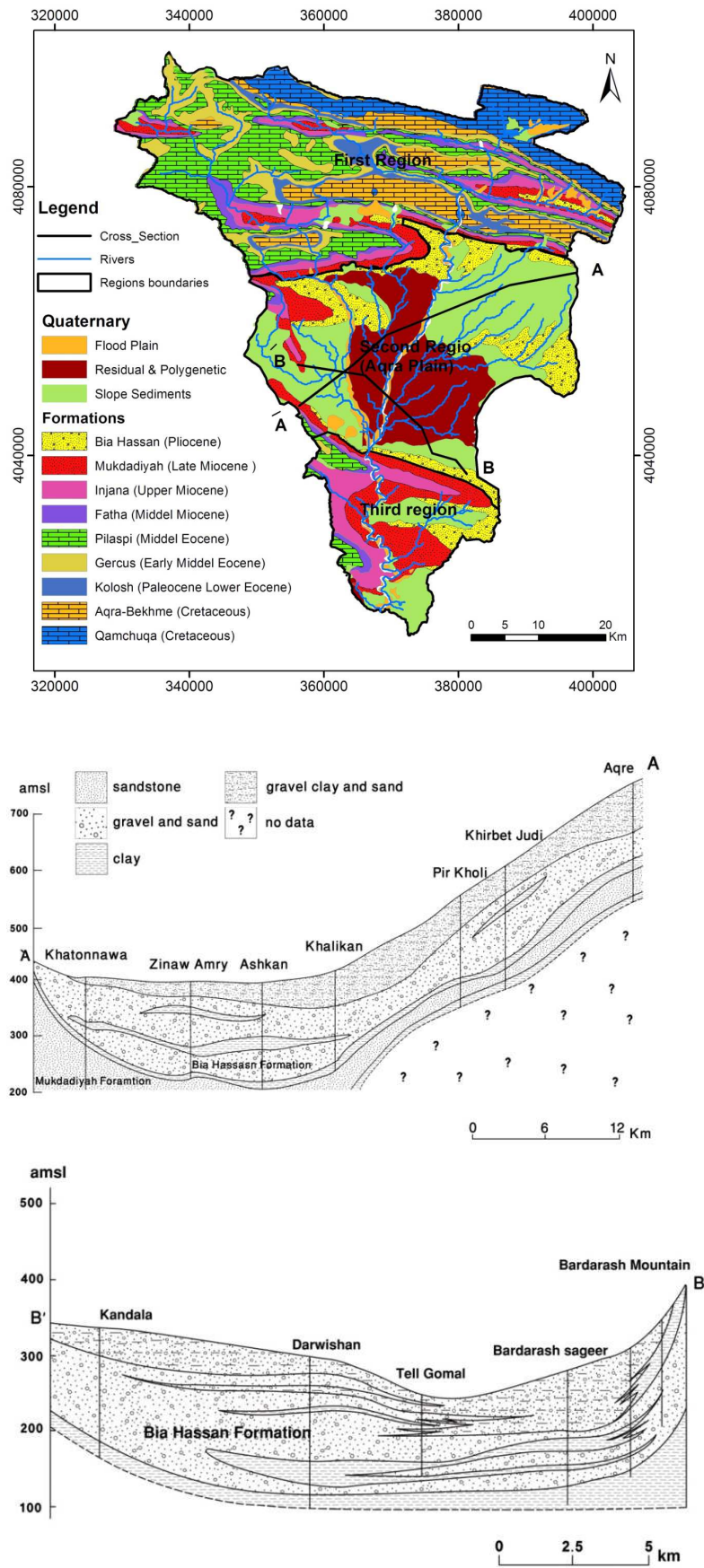


Fig. 2: Geological map and hydrogeological profiles (AA and BB) at Aqra plain (Jassas and Merkel 2015)

3. Methodology

Data required for this study consists of hydrogeological and physical properties. Hydrogeological properties include the topographic map extracted from the digital elevation model (DEM) with locations of boreholes and geologic formations. Physical parameters encompass transmissivity, recharge, aquifer thickness, and estimated pumping rates. Moreover, the model domain and boundary conditions were assigned using the geological and hydrological information.

Depths to groundwater at a number of wells were measured during 2011-2012 in two field trips (wet and dry season). Hydraulic properties and recharge were assigned depending on the pumping test conducted in the plain and were adjusted later on while calibrating the model. The calibration of the model was conducted for steady state by trial-and-error method. Then the model was validated using the baseflow measured by hydrograph analysis. In order to qualify the model sensitivity the analysis was used with respect to hydraulic conductivity, recharge, and conductance. Particle-tracking was used to show groundwater flow path patterns which could support future field investigation to determine the time travel of potential contamination sources.

3.1. Groundwater flow model design

To implement the groundwater simulation of Aqra Plain aquifer, three-dimensional finite difference numerical models were developed using MODFLOW-2000 with the graphical user interface Visual Modflow version 4.2. The MODPATH package was used for tracing groundwater flow-paths, and Zone Budget package (Harbaugh 1990) for calculating water balance. Because of the heterogeneities (lateral variation) associated with the study area, several simplifications, generalizations, and assumptions were made to construct the regional-scale model. Depending on hydraulic head measurements which did not show significant differences, a single monolayer model was adopted in this study, because no data were available for a multilayer model. Due to the lack of time-series of field data like stream stage data and seasonal groundwater level measurements it was impossible to build a transient model.

The horizontal hydraulic conductivity (K_h) was calculated depending on the thickness and transmissivity (T) in 6 pumping test locations distributed in the plain (Fig.1). Hydraulic conductivity was optimized by the trial-and-error method. The vertical conductivity (K_v) was supposed to be less by one order of magnitude. The digital elevation data of SRTM 90 was used to define the surface elevation.

ArcGIS Geostatistical Analyst tool was used to estimate the thickness of the unconfined aquifer layer from the lithological description of 210 wells, 58 of them penetrate the entire thickness of the aquifer. The boundary of Aqra plain aquifer was delineated following the water divide and the contact between Bia Hassan and Mukdadiyah formations. Then, the study area was horizontally discretized $101 (x) \times 101 (y)$ (10201 horizontal grid cells), with square cells of 500 m (Fig.3). Maximum and minimum thickness of the model was 250 m, 30, respectively, and to increase the resolution, the model was vertically discretized in 7 layers (total of 71,407 grid cells of which 29,960 were active). To simulate the average behaviour in the period 2011 to 2012 the model is run in steady-state regime.

3.2. Boundary conditions

The modeled study area is bounded in the north and north-west, south and west by the Aqra Mountains, Bardarash and Maklub Mountains, Sinjar Mountain, respectively (Fig. 1). This means, that Aqra plain is completely bounded by water divides and thus no-flow boundaries (Fig.3), which separates it from adjacent basins. The divide follows a ridge line around the plain, crossing the plain only at the point when Alkhazir and Gomal rivers cross Aqra and Bardarash mountains. The base of the aquifer was defined as no-flow boundary, consistent with the late Miocene clay layer, which underlay the unconfined aquifer.

The perennial Alkhazir River which crosses the middle part of the plain and its main tributary Gomal River was considered as a river boundary condition (Fig 3). The relation between the aquifer and rivers depends on the hydraulic gradient, where the river feeds the aquifer upstream and vice versa downstream. As there was no data available on rivers conductance, an arbitrary value was used, to ensure a good contact between the river and the aquifer, and to be consistent with the high permeable sediments of the river bed which consists mainly of sand and gravel. Leakage from the river bottom is controlled by river conductance which represents the resistance to flow between the surface water body and the ground water. The conductance for Alkhazir and Gomal Rivers in m^2/day was calculated as:

$$C = K \times L \times W/M \quad (1)$$

where, C is the river conductance (m^3/s), L is the length a cell (500 m); W is the width of the river in m; M is the thickness of a river bed in m; and K is the hydraulic conductivity of the riverbed material in m/s. The width W, the thickness M, and bed elevation and water level were obtained from Duhok irrigation directorate/Aqra department and are checked in the field.

3.3. Estimation of the annual groundwater pumping rate and recharge

Groundwater is considered the main water supply in the plain, so the pumping rate of the existing wells is another important boundary condition for the model. According to data provided by Aqra drilling well department, ministry of water resources, there are more than 400 wells in Aqra plain pumping water from the unconfined aquifer; most of them are for domestic and the rest for irrigation use. Unfortunately there is no accurate statistics about the amounts of extracted groundwater. Therefore, for this model the pumping rate (the net consumed groundwater) was estimated depending on the actual evapotranspiration (ET_a) in dry season. In this season groundwater is considered the solely source used to irrigate summer crops.

The ET_a in the growing season (Jun., Jul., and Aug.) was calculated by means of SEBAL (Surface Energy Balance Algorithm for Land) to be 18 mm during 2006 (Jassas, Kanoua and Merkel 2015). However, not all water used for irrigation is pumped from the unconfined aquifer, because some of irrigation water is pumped from the deep confined aquifer. Therefore, 50% of ET_a (9 mm/a) which equal to $9.6 \times 10^6 m^3$ was assumed to be pumped and consumed from the unconfined aquifer. The population in the catchment is about 25000 (information from municipal districts) and water per capita consumption in rural communities is about 170 L/day (General Directorate for Water Resources Management 2006), thus the annual domestic consumption is equal to $1.5 \times 10^6 m^3/y$. Therefore, the total amount of annual agricultural and domestic consumption was estimated to be $11 \times 10^6 m^3$.

The integrated annual recharge was estimated by water balance approach through applying two methods: water table fluctuation (WTF) and hydrograph analysis to be in average of 131 mm/y (Jassas & Merkel 2014). Therefore, this recharge value was assigned in the model. Regarding spatial distribution of recharge it was assumed that recharge is higher at the mountain front through the high permeable Pliocene sediments (recharge windows) and along ephemeral and perennial rivers courses.

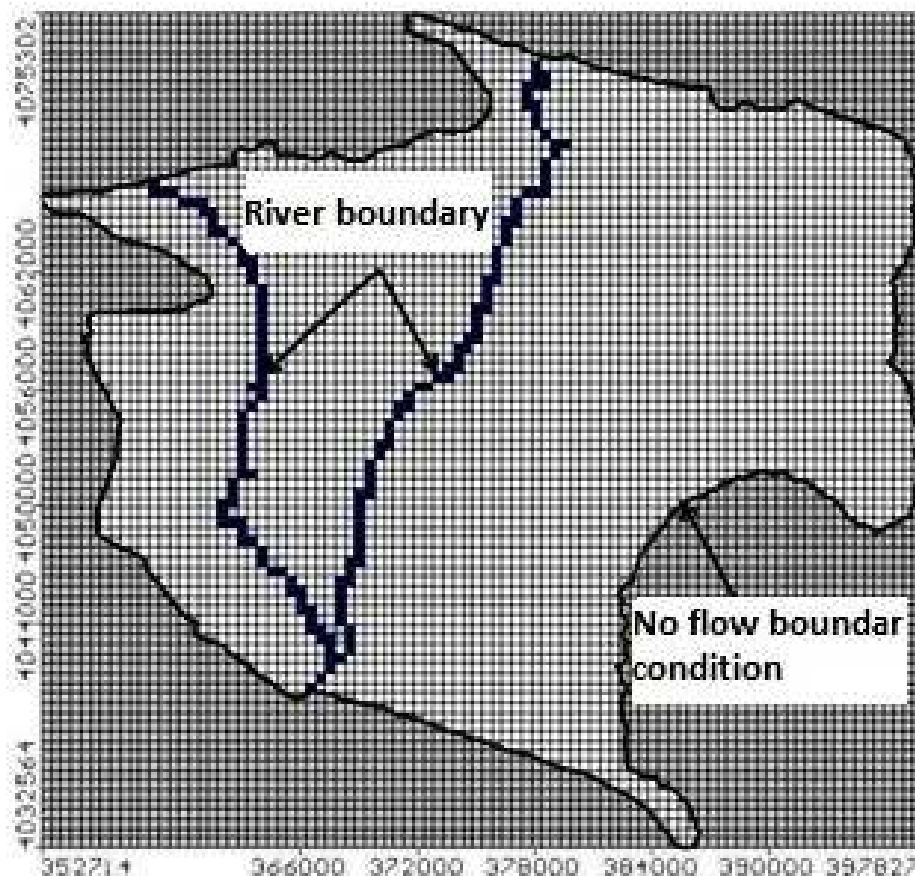


Fig. 3: The model grid and model boundary conditions of Aqra plain aquifer system

4. Results

4.1. Model calibration

Model calibration was performed for the average groundwater levels measured in dry season (Oct. 2011) and wet season (Apr. 2012) for 53 observation wells distributed all over the plain. The calibration was done by comparing the values calculated by the model with the corresponding observations. The calibration procedure involves manual trial and error adjustments of the most sensitive parameter (hydraulic conductivity, recharge, and conductance) within reasonable ranges until reaching the minimum residuals between computed and observed heads. Figure 4 shows the results with a correlation coefficient of 0.986, an Absolute Residual Mean Error (ARME) of 5.59 m and a Root Mean Squared Error (RMSE) of 7.23 m. The results show that the model is adjustable to the natural conditions by manual calibration.

4.2. Validation

A good match between measured and simulated water heads does not prove the model validity, because the solution is non-unique, and the model may include compensating errors (Konikow and Bredehoeft 1992). In light of this fact, other criteria have to be used as well. Model performance has to be evaluated e.g. by comparing the calculated annual baseflow at the outflow point of the model with the annual baseflow measured at the outlet of the Aqra plain during 2011-2012. The difference between measured baseflow ($189 \times 10^6 \text{ m}^3/\text{a}$) and simulated baseflow ($159 \times 10^6 \text{ m}^3/\text{a}$) is 16%. This dif-

ference seems to be acceptable if one takes into account the method used to measure the river discharge (Rating Curve method), and the percentage of error inherent in the baseflow separation method which depends on the arbitrary truncating of the stream discharge peaks considering the remaining discharge as baseflow (Wahl & Wahl 1988). Another option for validating a numerical model is checking the model budget which is described in the following chapter.

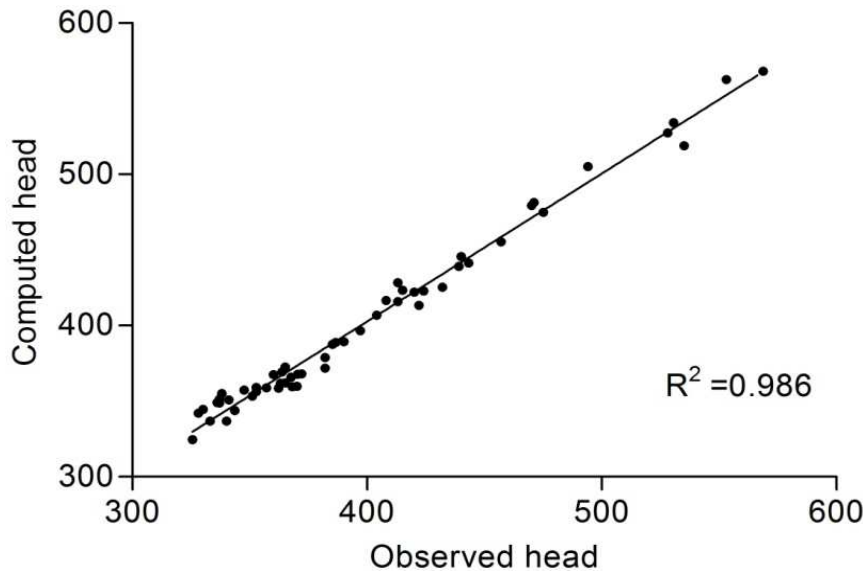


Fig. 4: Scatter plot of observed vs. computed head for the steady-state calibrated flow model (2011-2012)

4.3. Water budget

The water budget was checked by the volume of water leaving and entering the system. The cumulative water volume during the study period of the calibrated model (2011 to 2012) is from two major sources: recharge from precipitation and stream leakage. As cumulative volume, the annual direct recharge from precipitation accounts for about 35% ($60 \times 10^6 \text{ m}^3$) and rivers leakage accounts for about 65% ($111 \times 10^6 \text{ m}^3$). Groundwater discharge into the river as a baseflow is 92% ($159 \times 10^6 \text{ m}^3$) and the discharge from the pumping wells is about 8% ($10.5 \times 10^6 \text{ m}^3$). According to the no flow boundary conditions, the groundwater inflow is 0% (closed system). Because the depth to the groundwater is 19 m in average evapotranspiration from the water table was neglected. The mass balance error for simulation of about 0.0001% is considered acceptable

4.4. Sensitivity analysis

Sensitivity analysis is normally used to quantify the uncertainty in the calibrated model caused by uncertainty in the estimated aquifer parameters and considered as an essential step in modeling to evaluate the reliability of the developed model (Anderson & Woessner 1992; Chiang & Kinzelbach 1998). In order to evaluate the model sensitivity to any changes in the model input parameters, the final result of the calibrated model were used for a sensitivity analysis. The procedure used in this analysis depends on changing only one input parameter and keeping the rest fixed. The purpose was to assess the groundwater response to any change in the hydraulic parameter and which of them have the highest effect on the hydraulic head. Here the hydraulic conductivity (K), river conductance and groundwater recharge (R) were changed stepwise from the calibrated values and the Residual Mean Standard Error (RMSE) was noted. The multiplying factor ranged from 0.4 to 1.6 and the result is shown in Figure 5. The variation of hydraulic heads is highly dependent on variation of hydraulic conductivity more than the groundwater recharge and rather slightly on river conductance.

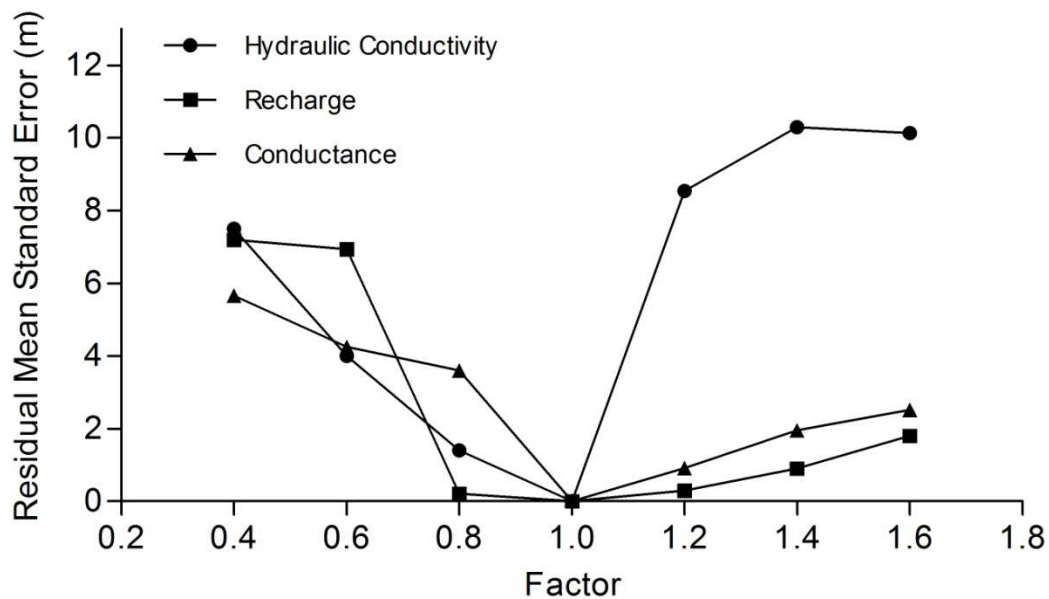


Fig. 5: Sensitivity analysis results for hydraulic conductivity, recharge, and conductance

4.5. Particle-tracking simulations

Particle tracking presents path lines and travel times for advective transport without considering diffusion, dispersion and retardation due to chemical reactions. Simulations were performed on steady state conditions in both forward and backward mode. The first simulation tracked the recharged water at the mountain front to estimate the travel time from recharge to discharge area. The second simulation was to estimate contaminant's travel time to the extraction wells. In the first simulation, the particles were located in the potential recharge areas in the north, west and east edges of the plain and the particles were tracked forward along the flow paths. In the second simulation, 25 particles were assigned in the center of each abstraction well for best path line visualization and the particles were tracked backward. Based on the geological logs, the effective and total porosity was assumed for both simulation to be 15% and 30%, respectively.

Particles released in the recharge areas travelled down gradient to reach the discharge areas along Alkhazir River near Kelekchi district. Figure 6 shows flow-paths after 200, 600, and 1000 years (Fig. 6). The discharge area determined by the simulation is consistent with the area at which many springs feed Alkhazir river course. Travel times (residence time) are in the range 200 - 1000 years for particles released at the plain boundaries. However, the travel time is low at the center of the plain and the flow path lines tend to converge. The residence time estimated by simulation is consistent with the average residence time measured by radioactive carbon (^{14}C) for water picked up from the baseflow water at the discharge area, where the carbon activity was 80.6 pmc and the corrected age using $\delta^{13}\text{C}$ model was 950 year (Jassas and Merkel 2015).

To check the origin of potential pollutants, the reverse tracking was conducted by placing the particles in the center of the extraction well and backward tracking. The particle distance from the pumping well after 10, 200 and 500 years are shown in Figure 6. The particles located in the wells at the northern parts moved about 10,000 m from the cell center towards the contamination sources origin after 500 years, while the particles located in the wells at the central parts moved more than 13,000 m after 100 years. The stagnation in the particle trajectory at the mountain front may be the result of the low permeability of the compacted rocks in this area.

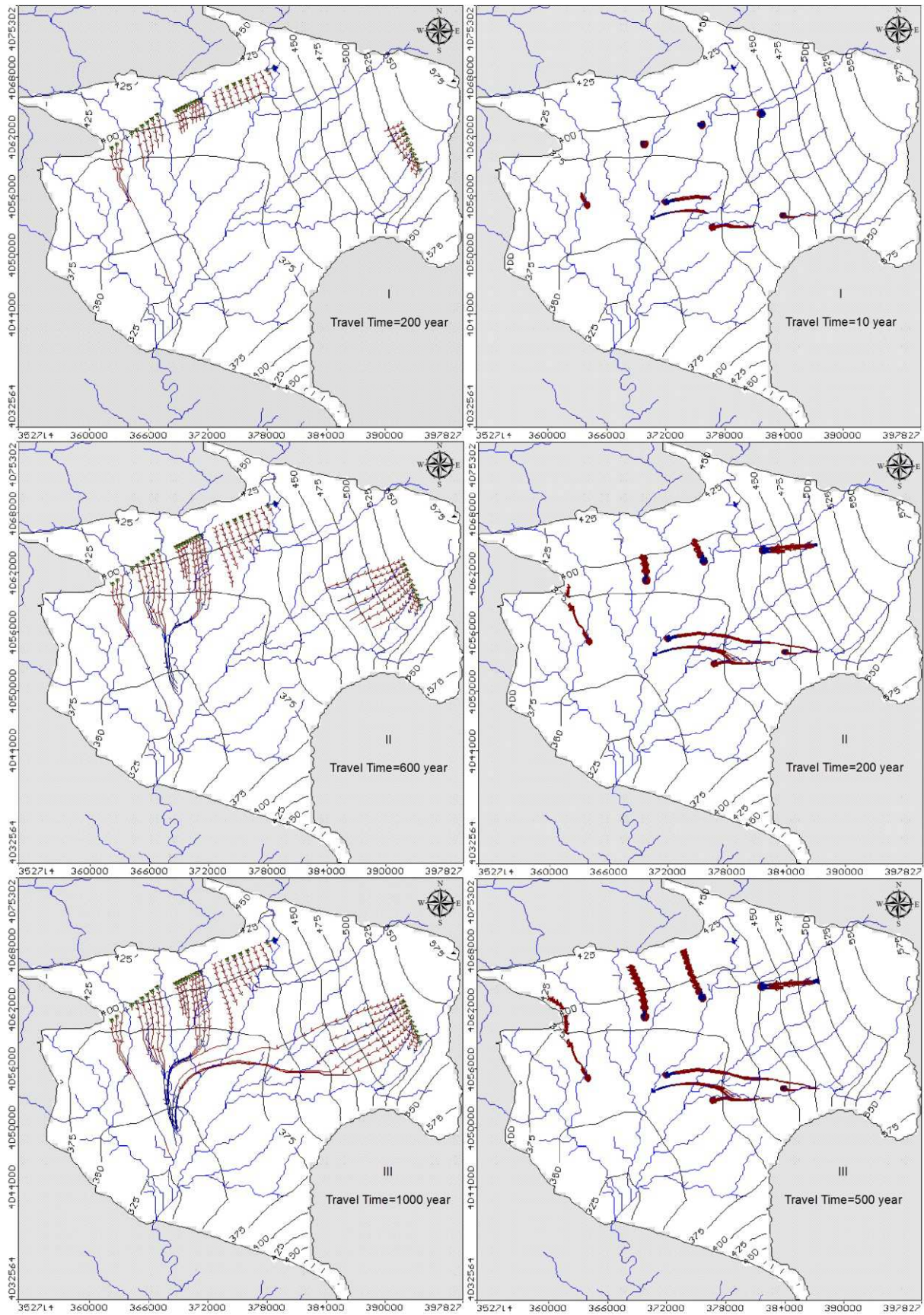


Fig. 6: Flow paths simulation of particles initially placed at: 1. left, potential recharge areas cells for forward tracking particles (travel time of 200 years (I), 600 years (II), and 1000 years (III)); 2. right, extraction wells cells for backward tracking (travel time of 10 years (I), 200 years (II), and 500 years (III))

4. Conclusions

This study is considered the first attempt to model the unconfined aquifer in this region by using a combination of geo-statistics plus hydrogeological and hydrological modeling to approximate the real field conditions. The steady state 3D model of the Aqra plain unconfined aquifer shows the interaction between river and groundwater, and that the indirect recharge as water losing streams (river leakage in) represents the largest share of the total recharge (65 %) in the plain and the direct recharge represent 35 %. Also the result shows that the aquifer is under sustainable use and the leakage from the aquifer to the river (baseflow) represents 92 % of the system output and outflow to wells represent 8 %. The horizontal hydraulic conductivity, obtained from the calibrated model, ranges between 8.5×10^{-4} m/s in the plain centre to 5×10^{-6} m/s in the plain margins. The aquifer model is as expected more sensitive to hydraulic conductivities than recharge and river conductance.

MODPATH results shows that migration of potential pollutants from the plain edges to the discharge point downstream may take 200-1000 years, and the stagnation in the mountain front is due to the low permeability of the compacted rocks. The particles in reverse tracking mode in the central plain shows that the pollutions transport speed into the extraction well is five times more than the transportation speed in the mountain front area. Therefore, care should be taken to reduce the potential industrial and agricultural pollution releases near the extraction wells in the center of plain.

Based on water budget results, the aquifer has a high capacity for water extraction and is able to meet the water demands in the plain. However, one should take in consideration uncertainties in a groundwater flow analysis.

Acknowledgments

This work was funded by the German Academic Exchange Service (DAAD), and supported by TU Bergakademie Freiberg, Geological Survey of Iraq (GEOSURV) and the Iraqi Ministry of Higher Education and scientific research.

References

- Al-Basrawi NH (2006) Hydrogeological and hydrochemical study of Erbil Quadrangle (NJ – 38 – 14), scale 1:250000. int. rep. no. 3037, Baghdad.
- Al-Jiburi HK (2007) Hydrogeological and hydrochemical study of Mosul Quadrangle (NJ-38-13), scale 1:250000. , int. rep. no. 3058., Baghdad.
- Al-Sam S. and Hanna F (1981) Evaluation of Groundwater Resources in Al-Khazir Gomal Basin, int. rep. no.1270., Iraq-Baghdad.
- Anderson MP and Woessner WW (1992) Applied groundwater modeling: Simulation of flow and advective transport., San Diego: Academic Press.
- Chiang, W.-H. & Kinzelbach, W., 1998. Processing Modflow A Simulation System for Modeling Groundwater Flow and Pollution,
- Director General Of Irrigation (2012) Discharges for Alkhazir River at Manguba Gauge Station.,
- General Directorate for Water Resources Management (2006) Forecasting Demand for Municipal and Rural Water Supplies and Wastewater Services, Baghdad.
- Harbaugh A (1990) A computer program for calculating subregional water budgets using results from the U.S. Geological Survey modular three-dimensional ground-water flow model. U.S. Geol Surv Open-File Rep 90-392,

- Harbaugh AW, Banta ER, Hill Mc, McDonald MG (2000) MODFLOW-2000, the US Geological Survey modular groundwater model—user guide to modularization concepts and the groundwater flow process. US Geological Survey Open-File Report 00-92,
- Jassas H and Merkel B (2014) Estimating Groundwater Recharge in the Semiarid Al-Khazir Gomal Basin, North Iraq. *Water*, 6(8), pp.2467–2481.
- Jassas H, and Merkel B (2015) Investigating groundwater recharge by means of stable isotopes in the Al-Khazir Gomal Basin, northern Iraq. *Environmental Earth Sciences*, 1–14. doi:10.1007/s12665-015-4013-7
- Jassas H, and Merkel B (2015) Assessment of hydrochemical evolution of groundwater and its suitability for drinking and irrigation purposes in Al-Khazir Gomal Basin, Northern Iraq. *Environmental Earth Sciences*, 1–17. doi:10.1007/s12665-015-4664-4.
- Jassas H, Kanoua W, and Merkel B (2015). Actual Evapotranspiration in the Al-Khazir Gomal Basin (Northern Iraq) Using the Surface Energy Balance Algorithm for Land (SEBAL) and Water Balance. *Geosciences*, 5(2), 141. doi:10.3390/geosciences5020141
- Jassim SZ and Goff JC (2006) *Geology of Iraq* first edit., Prague: Dolin.
- Konikow LF and Bredehoeft JD (1992) Ground-water models cannot be validated. *Advances in Water Resources*, 15(1), pp.75–83.
- Krasny J (1983) *Hydrogeology and Hydrochemistry of the Foothills zone*, Baghdad.
- Mukherjee A, Fryar A and Howell P (2002) Regional hydrostratigraphy and groundwater flow modeling in the arsenic-affected areas of the western Bengal basin, West Bengal, India. *Hydrogeology Journal*, 15(7), pp.1397–1418.
- Pollock DW (1994) User's Guide for MODPATH/MODPATH-PLOT, Version 3 e a Particle Tracking Post-processing Package for MODFLOW, the U.S. Geological Survey Finite-difference Groundwater Flow Model. U.S. Geological Survey Open-File Report 94-464, 120 pp.,
- Sissakian VK. and Galib AA (1995) *The Geology of Mosul Quadrangles sheet NJ-38-3*, Scale: 1:250000, GEOSURV, Baghdad.,
- Stevanović Z, Adrian and Aleksandra M (2009) New Insights into Karst and Caves of Northwestern Zagros Northern Iraq. *Acta Carsologica*, 38(1), pp.84–96.
- Stevanovic Z and Iurkiewicz A (2004) *Hydrogeology of Northern Iraq, Vol. 2. General hydrogeology and aquifer systems*, Rome, Italy.
- Stevanovic Z and Marković M (2004) *Hydrogeology of Northern Iraq, Vol. 1. Climate, hydrology, geomorphology and geology*, Rome, Italy.
- Wada Y, Van Beek L, Van Kempen CM, Reckman J, Vasak S and Bierkens M (2010) Global depletion of groundwater resources. *Geophysical Research Letters*, 37(20), p.L20402.
- Wahl KL and Wahl TL (1988) Effect of regional groundwater level decline on streamflow in the Oklahoma panhandle. In: *Proceedings of the symposium of water resources Assoc.*

Has the water supply network of Sebestia been connected to that of Nablus?

Sabri, Raghid	Department of Hydrogeology, Institute of Geology, Technische Universität Bergakademie Freiberg, Gustav-Zeuner-Str. 12, 09596 Freiberg, Germany; Email: raghid_sabri@yahoo.com
Merkel, Broder	Department of Hydrogeology, Institute of Geology, Technische Universität Bergakademie Freiberg, Gustav-Zeuner-Str. 12, 09596 Freiberg, Germany; Email: merkel@geo.tu-freiberg.de
Tichomirowa, Marion	Institute of Mineralogy , Technische Universität Bergakademie Freiberg, Brennhausgasse 14, 09596 Freiberg, Germany; Email: tichomir@mineral.tu-freiberg.de

The nowadays water supply system in Nablus-Sebestia is still based on the same springs that were supplying the two cities with domestic and agricultural water for the past 2000 years. The main springs in the area have been used since Roman times. The question addressed in the present study is whether there has been a connection between the ancient water supply network of Nablus city (Flavia Neapolis) to support the water supply network in Sebestia 12 km northwest of Nablus.

To answer this question, geochemical investigations were performed in the study area. Water and carbonate samples (sinters) were collected from 12 springs, one tunnel, and one aqueduct. Some of the springs were rehabilitated recently and the carbonate sinters have been removed. As opposed to some of the springs, the aqueducts and tunnels still exist and carbonate sinters can be found on them. The tunnel and the aqueduct are located within Nablus city. Laminated carbonate sinters and water samples were analyzed using Thermal Ionization Mass Spectrometry for determining the Sr isotope ratios. For the laminated carbonate samples, 2–5 sample points from the laminated sinters were analyzed for each sample.

The Sr isotope ratios for water and carbonate from the springs showed at least two sources of Sr in groundwater and these two sources differ significantly from each other. Based on the Sr isotope ratio for carbonate samples from the tunnel and the aqueduct one can speculate that in different time periods the two structures were fed by both the Nablus and the Sebestia springs.

The Sr isotope ratios for water and carbonate samples from Sebestia differ significantly in two of the Nablus springs. Thus, based on the present study, it is obvious that the tunnel and the aqueduct were fed by more than one type of water. On the other hand, there is no evidence that Ras al Ein or Qaryon have been used in the Roman time to feed the water network of Sebestia.

Keywords: Nablus, Sebestia, Ijnisinya, springs, aqueducts, carbonate, Sr isotope ratio

1 Introduction

1.1 Background

Palestine is a very complex place because of political, social and ecological reasons. The limited availability of natural resources presently raises the question on how the people could survive in one of the oldest civilizations. The archeological settings are very complicated as several elements are missing. For example archeological sites have been demolished due to poor control and low interest of the successive authorities.

On the other hand, however, archeology and human interaction with the environment are very important topics in this area. As the country is neither politically, nor environmentally, socially or economically sustainable, there is a need to read in the past for improving the future.

1.2 Aim of the study

Field studies, digging and archeological excavation are difficult in this area and will encounter political problems. While geo-archeology is an approach used to bridge the gap between archeology and physical science (Ruddiman, 2013), in this study it is used to overcome the above-mentioned difficulties. So, the aim of this work is to answer some archeological questions through geochemical investigations.

2 Study area

Nablus, Sabestia and Ijnisinya are ancient Palestinian locations in the north-western West bank belonging to Nablus Governorate (Figure 1). The earliest evidences of Nablus city history are from the Iron Age, the settlement started in the Hellenistic era 331 B.C. (Fanni, 1999) and developed into a city in 27 A.D. (Fanni, 2007). Sabestia was constructed by Herod in 27 B.C. Both cities were connected with roads (Chancey & Porter, 2001).

Currently, Nablus Governorate is the second largest Governorate in the West bank with a population of about 377 thousand inhabitants (PCBS, 2014). Nablus city is the largest city in the Governorate with 146,493 people, Sabestia is a village with 3,036 inhabitants and Ijnisinya is a small village with 587 inhabitants (PCBS, 2015a).

Nablus Governorate suffers from a deficit in water suitable for domestic use. In 2013, this deficit was estimated to account for 9.1 million m³ (PCBS, 2015b). Despite the present water shortage, the area has a sophisticated ancient water system. Until now, the connection between parts of this system has not been clear. In the course of this article the present findings will be explained.

2.1 Ancient water system

The water supply system in Nablus and Sabestia is still based on the same springs that have been supplying the two cities with domestic and agricultural water in ancient times. Some of the springs were rehabilitated recently and the carbonate deposits (sinters) have been removed. In addition to the springs, the water aqueduct and the tunnels are still available as part of the heritage system.

One of the open questions about the ancient water system in Nablus city is whether there was a connection between the water networks in Nablus and Sabestia (Frumkin, 2002). Crowfoot also mentioned the possibility of connections between the water conduit in Ijnisinya and Sabestia (Crowfoot, 1966). The main springs in Nablus are considered and dated as Roman springs. The Sabestia springs Harun and Ijnisinya are also considered as Roman springs (Crowfoot, 1966). All this springs have the same entrance structures and could therefore have a chronological connection. Yet,

Harun springs also have several tunnel connections similar to the tunnel found in Nablus below the Roman cardo. So, the question arises whether there has been a connection between the water system in Nablus, Sebestia, and Ijnisinya.

The springs, the aqueduct and the tunnel entrance locations are shown in Figure 1. Unfortunately, the total length of the aqueducts and the tunnel is neither documented nor excavated, so only the sampling locations appear in map. Yet the potential connection between the springs (Qaryon, Ras Al Ein and Harun) and the tunnel path starting from Dafna spring as suggested in literature (Fanni, 1999; Frumkin, 2002) are shown in Figure 1. For simplification, in the map it is drawn as straight line, which was probably not the case in reality (Figure 2) shows the curves in the tunnel.

Harun spring consists of an 80 m long channel; 30 m before the end of the channel there is a room with an inspector chamber similar to Ras al Ein spring (Frumkin, 2002) and Ijnisinya. The water seeps into the room via fractures. The room used to be connected with another water channel that brought the water from another unknown source (Crowfoot, 1966). Crowfoot suggested that Harun spring installation was linked either to Ijnisinya or to the water system in Nablus based on traces of aqueducts (Crowfoot, 1966). Frumkin suggested that Harun spring installation was linked with Ras al Ein spring because of the similarity of the structures and the aqueducts between the two cities. Currently Sebestia city depends on the water sources coming for the water network and Harun spring is used for irrigation.

The tunnel portal was found in the 1970s. According to archeological findings, it is dated to the 2nd century A.D. (Fanni, 1999). As mentioned before, the total length has not been studied, but it was suggested that the water from Dafna spring had been feeding the tunnel (Fanni, 1999). Dafna is located at 560 masl; the tunnel entrance is located at around 560 masl, too. From the entrance 74 steps direct downwards to the tunnel (Fanni, 1999). Going to the east it is possible to reach one shaft well (Dullab) located at 16 m below the street level. The tunnel dimension is variable; in the beginning walking is easy (2 m × 0.6 m); then it becomes difficult to walk due to the smaller dimensions (1.3 m × 0.6 m).

The hypothesis is that six shaft wells tapped the tunnel in the area of Nablus starting from Dafna. Figure 3 shows the Dullab shaft well that is near the entrance of the tunnel. It is not possible to reach the spring Dafna from the tunnel and the hypothesis is based on the presence of successive wells (Fanni, 1999; Frumkin, 2002). On the other hand, at Qaryon spring several tunnel installations were found but no link to any water network system could be determined (Frumkin, 2002). This is why in this article it was also investigated whether only water from the Dafna spring was feeding this tunnel.

So, to answer these questions geochemical investigations of the water system were conducted. The components of the water system include: 12 springs, one aqueduct and a water tunnel. The 12 springs are located in Nablus, Sebestia and the villages nearby. As shown in Figure 1, the tunnel is situated between three springs: Qaryon, Ras al Ein and Dafna, whereas the aqueduct (Wadi Tufah) is located near Beit Alma and Al Subyan springs.

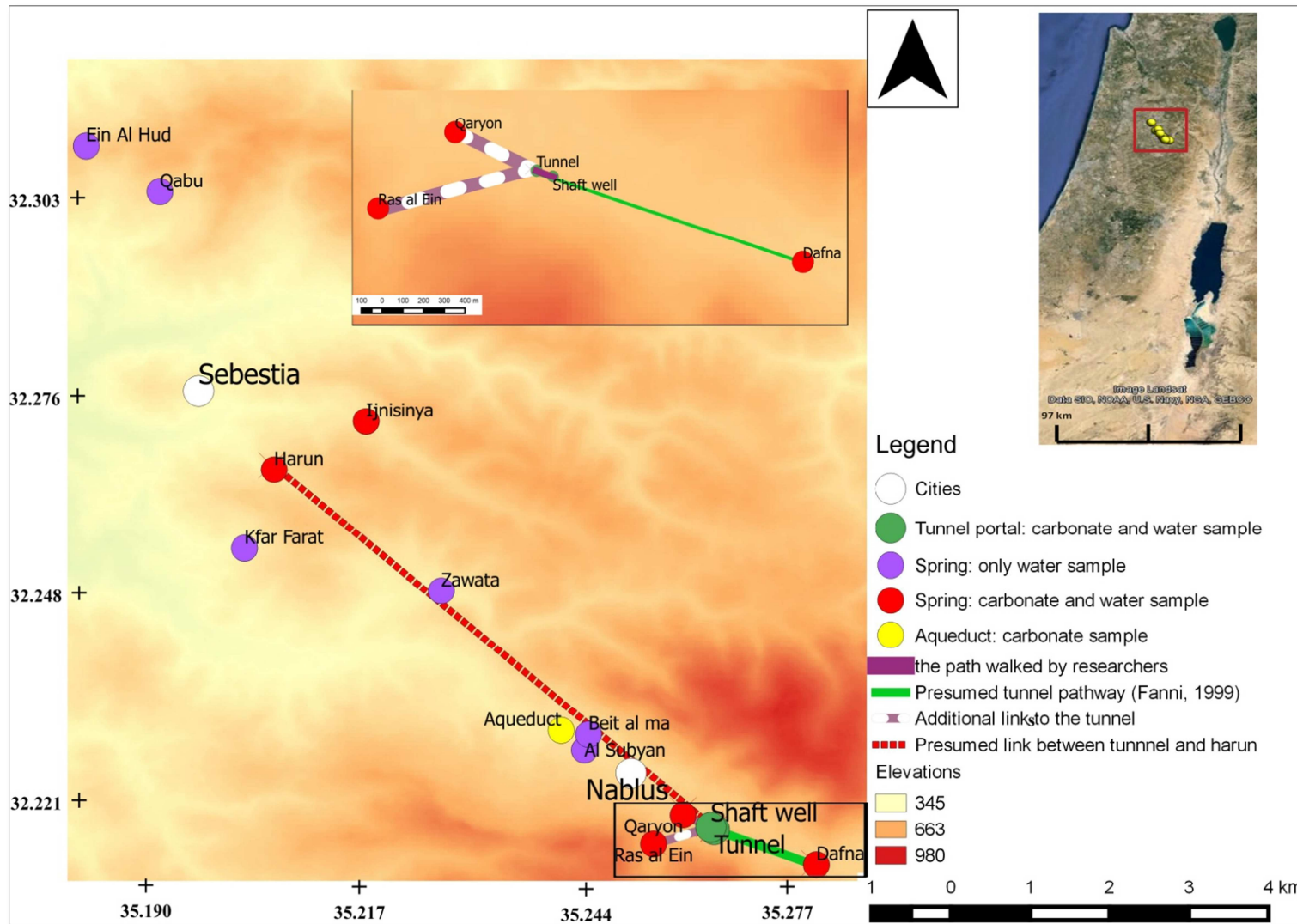


Figure 1: DEM SRTM 90 m resolution (USGS) with sampling location generated by QGIS, the clipping on the top right gives an overview of the Area Palestine location of the study area (Google earth map 2013 Landsat image)



Figure 2: Different cross sections in the tunnel, left showing the tunnel path curved



Figure 3: Dullab Shaft well in the tunnel ca. 100 m to the east from the tunnel entrance (looking upwards)

3 Methodology

Water and carbonate samples were collected in the region of interest. As mentioned before, carbonate sinters are missing at some springs because they have been removed recently due to maintenance works. So, sampling was also dependent on availability. Table 1 below lists the sample types and details on the sampling locations. For all water samples taken, the in-situ parameters pH, temperature, dissolved oxygen, redox potential and electrical conductivity were measured using WTW instruments.

Table 1: Sampling points and corresponding sample types

Sample names	Location of the sampling spots		Elevation in meters above sea level	Sample type	
	Eastings	Northings		Water	Carbonate sinters
Springs:					
Dafna	35 16 678	32 12 806	560	×	-----
Ras al Ein	35 15 21.60	32 12 55.86	620	×	×
Qaryon	351535.7	32 13 8.52	470	×	×
Al Subyan	35 14 811	32 13 685	474	×	-----
Beit al ma	35 14 842	32 13 802	560	×	×
Zawata	35 13 657	32 14 944	412	×	-----
Kfar Farat	35 12 081	32 15 293	416	×	-----
Harun	35 12 306	32 15 927	449	×	×
Ijnisinya	35 13 055	32 16 315	445	×	×
Ein Al Hud	35 10 845	32 18 323	478	×	-----
Qabu	35 11 406	32 18 176	503	×	-----
Tunnel	35 15 847	32 13 057	560 (entrance level)	×	×
Aqueduct Wadi Tufah	32 13 50	35 14 37	450	-----	×

The water samples were analyzed using Thermal Ionization Mass Spectrometry (TIMS, Finnigan MAT 262) for determining the Sr isotope ratio; NBS 987 standard was used with an external reproducibility of ± 0.00005 . The external reproducibility was used as error because it was higher than the internal error of the measurements.

An ICP-MS XSeries-2 Thermo Scientific instrument was used for determining the element concentration in the water samples. Internal standards (5 mg/L Ge, 1 mg/L Rh and 1 mg/L Re) were used to reduce the matrix effect. The reproducibility was 5%. Standard or collision mode was used depending on the manufacturer's recommendations for the measured element.

In addition to that, ion chromatography (IC Metrohm) was used to analyze the cations (Li^+ , Na^+ , NH_4^+ , K^+ , Mg^{2+} , Ca^{2+}) using Metrohm column C4/100 and 2 mM HNO_3 plus 0.7mM dipicolinic acid as eluent and to analyze the anions (Cl^- , Br^- , NO_2^- , NO_3^- , SO_4^{2-}) using Metrohm A Sub A 15/150 /4.0 with 3 mM NaHCO_3 and 3.5 mM Na_2CO_3 as eluent. Total inorganic carbon was analyzed by non-dispersive infrared spectroscopy (LiquiTOC II).

For the spring water quality (1954-2009) data was collected from different sources: The Palestinian Water Authority database ("Spring water chemistry," 2011) the 'Nablus District Water Resources Survey: Geological and Hydrological Report' from February 1965 (Raferty, van Bellen, & al-

Markaziyah, 1965) and the monography ‘Nablus Spring Source of Life Through History’ 2015(Alawi, Al-Masry, & Messerschmid, 2015).

PHREEQC was used to calculate the saturation index of calcite, aragonite, dolomite, gypsum, and halite using the WATEQ4F database. Furthermore, K-means cluster, Mann-Whitney test and Box-and-Whisker plots were used for statistical analysis using STATGRAPHICS Centurion XVI version 16.1.11 and OriginPro 2015. QGIS Valmiera was used for to create fig. 1.

3.1 Carbonate samples analysis

To prepare a sample, it was cut along the growth axis, washed with deionized water and then polished (Dorale, 2004; Spötl & Matthey, 2006). Thereafter, each laminated layer was extracted using a ‘New wave micromill’ drill with the smallest bit diameter (0.5 mm). After each extraction the drill bit was cleaned with ethanol.

For the element concentration measurement, 5 mg of each extracted lamination layer were diluted in 100 μL HNO_3 and subsequently analyzed using ICP-MS.

For the Sr isotope ratio analysis, 2-5 laminations from each sample were selected. For the preparation of the samples it was recommended to wash the powder samples with weak acid to remove secondary carbonates (Bailey, McArthur, Prince, & Thirlwall, 2000; Li, Shields-Zhou, Ling, & Thirlwall, 2011; Ruppel, James, Barrick, Nowlan, & Uyeno, 1996). So, 10 mg of the sample were diluted in 1 mL 0.05 M HCl for 2 hours without heating; then the solutions were centrifuged and the supernatant was discarded. This procedure ensured a 40 % mass reduction of the sample. Then the residue was diluted in 1 mL 0.5 M HCl and subsequently analyzed using TIMS.

4 Results and discussion

The water chemistry of springs in the area is characterized by high Ca and HCO₃ contents. There is a seasonal variation in the water composition (Appendix 1-11), but in general the characteristics of the water do not change. As shown in Figure 4, the water in the tunnel -yellow triangles- has a chemical composition different from all other springs in the area because it is currently polluted with mixed groundwater and surface runoff water (Sabri, Merkel, & Tichomirowa, 2015). The calculation of saturation indices with PHREEQC indicates that calcite is oversaturated in the springs' waters (Table 2). This explains why carbonate has been deposited on the walls of the water supply structures.

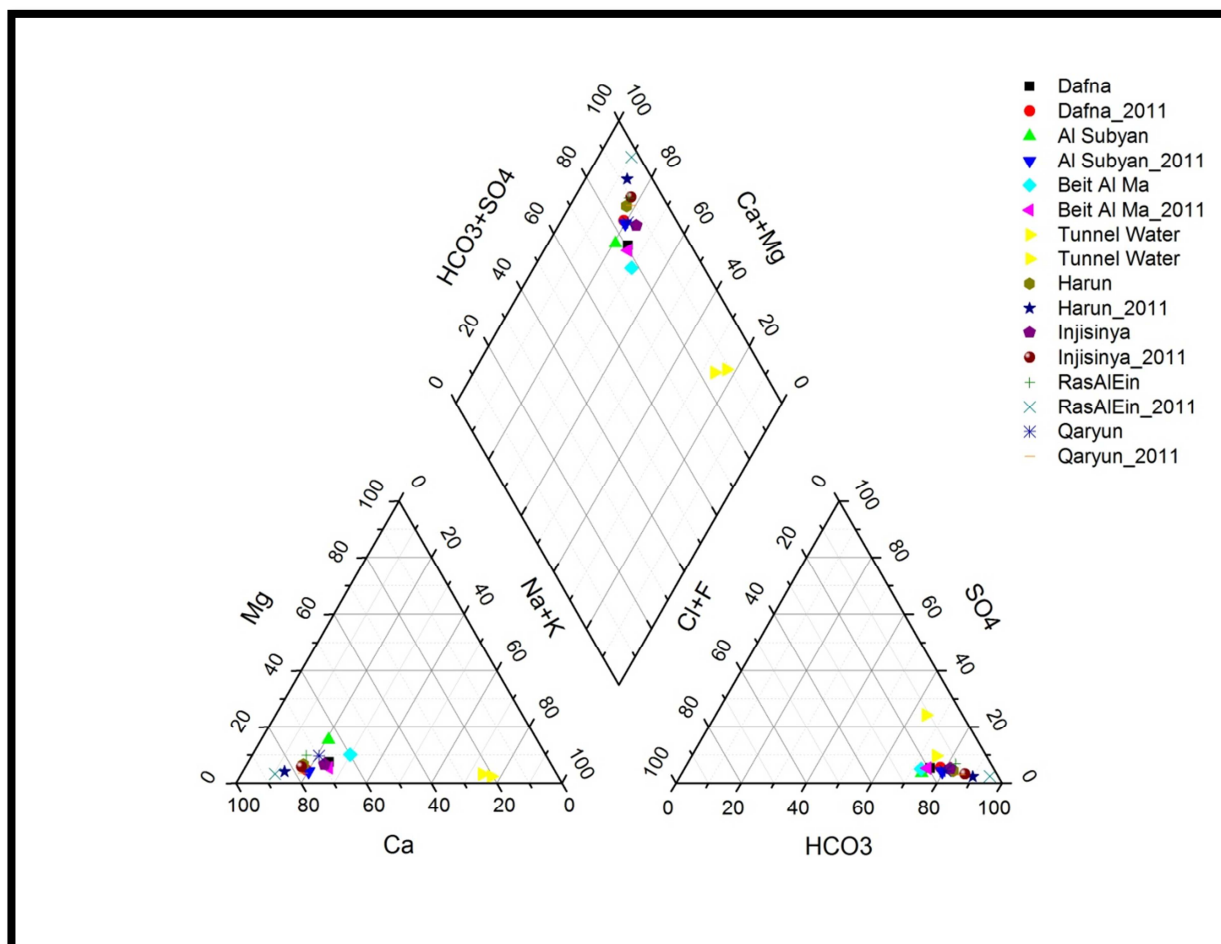


Figure 4: Mean composition of the sampled waters in the study area (1954-2009) and 2011

Table 2: Saturation indices for selected minerals in the springs

	<i>si_Calcite</i>	<i>si_Dolomite</i>	<i>si_Aragonite</i>	<i>si_Halite</i>	<i>si_Gypsum</i>
Dafna	0.2819	-0.3762	0.1333	-7.4522	-2.6614
Ras al Ein	0.0632	-1.0288	-0.0857	-8.2507	-3.2826
Qaryon	0.1507	-0.7784	0.0023	-7.6142	-2.9665
Al Subyan	0.8562	0.7401	0.7084	-7.1086	-2.5433
Beit al Ma	0.0277	-0.7582	-0.1199	-7.2256	-2.6988
Watertunnel	0.4803	0.3794	0.3322	-6.2141	-2.2482
Harun	0.2326	-0.5539	0.085	-8.2113	-3.2053
Ijnisinya	0.2211	-0.3903	0.0737	-7.7907	-2.9399

As mentioned before, Sr isotope ratios were determined for both, carbonate and water samples. Based on the current water quality and Sr isotope ratio values, the water supply systems in the area have at least two Sr sources because two groups, one with lower and one with higher Sr ratio, can be distinguished (values of 0.7079 ± 0.00005 and 0.7081 ± 0.00005 , respectively) as shown in Figure 5. K-means cluster analysis was done for determining potential Sr isotope ratio groups. Two clusters were defined as shown in Table 3. Cluster 1 includes the samples with higher Sr isotope ratios (0.7080 ± 0.00005) and cluster 2 includes the samples with lower Sr isotope ratio values (0.7079 ± 0.00005).

The results of the Mann-Whitney test indicate a statistically significant difference between the two clusters at the 95.0 % confidence level ($P= 0.01604$). These results are visualized by means of a Box-and-Whisker plot (Figure 6)

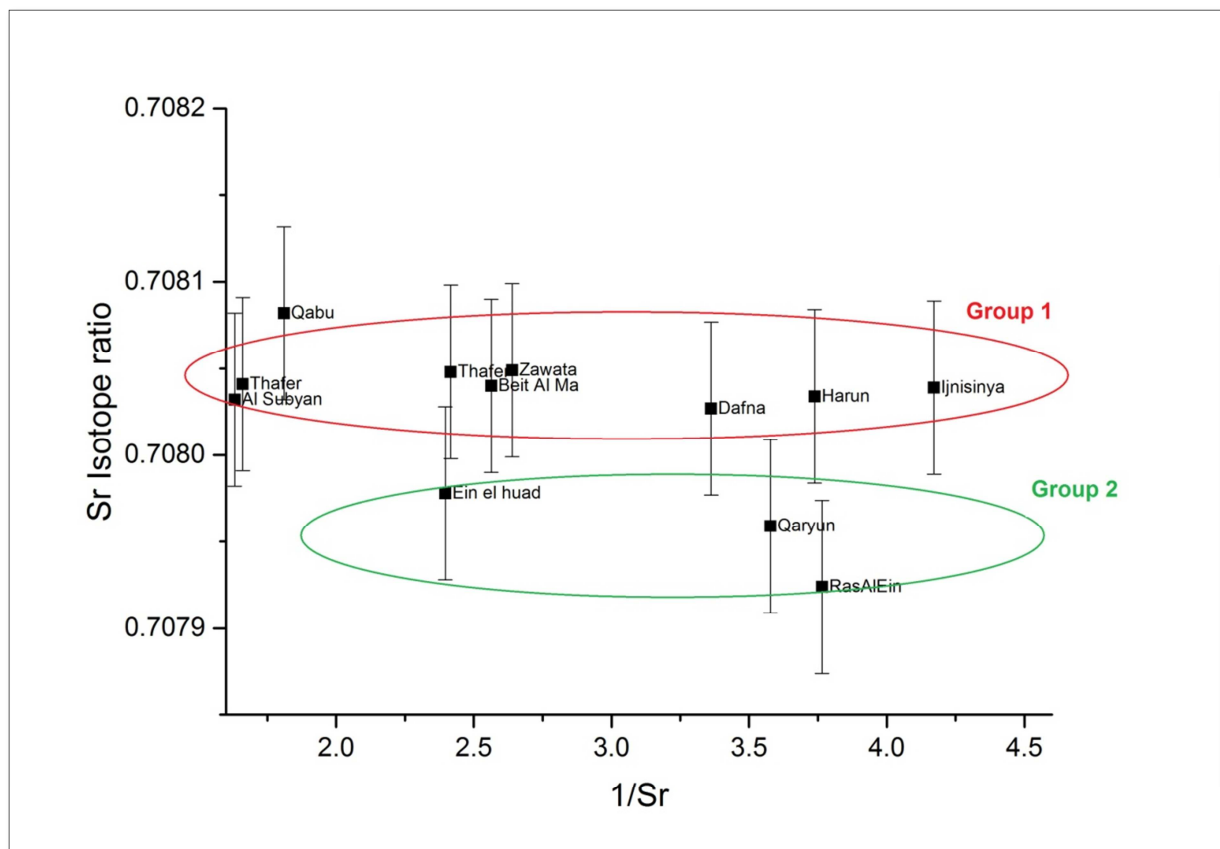
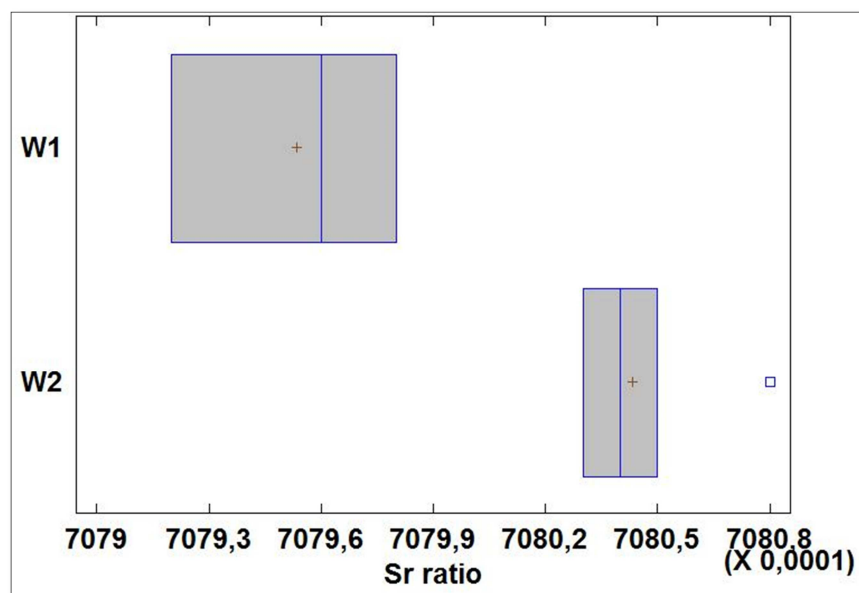


Figure 5: Sr isotope ratios of the springs, clustered into two groups by K-means cluster analysis. The error bars show the total error.

Table 3: Grouping of the water sources based on K-means cluster analysis of the Sr isotope ratio values

<i>Water source</i>	<i>Group number</i>
Dafna	1
Tunnel water	1
Ras al Ein	2
Qaryon	2
Al Subyan	1
Beit al ma	1
Zawata	1
Kfar Farat	1
Harun	1
Ijnisinya	1
Qabu	1
Ein Al Hud	2

**Figure 6: Box-and-Whisker plot of the Sr ratio values of water sample group cluster 1 and 2**

Based on the previous results, carbonate sinter samples from springs were clustered into two groups depending on the sampling location similar to clustering of water samples. So, the carbonate sample which was taken from spring group 1 is listed as group 1 and similarly for group 2. Carbonate samples taken from the aqueducts and the tunnel are not included in the analysis

Furthermore, the Mann-Whitney test showed a statistically significant difference between the two distributions of “water group” 1 and “carbonate sinter group” 2 at the 95.0 % confidence level ($P = 0.03577$). Similarly, “water group” 2 and “carbonate sinter group” 1 (P value = 0.0103), have significantly different Sr isotope ratios. As the carbonate sinter samples have the same Sr isotope ratio as the corresponding background water, there has probably not been a change of the water source during the sinters’ growth. This is shown graphically by the Box-and-Whisker plot in Figure 7.

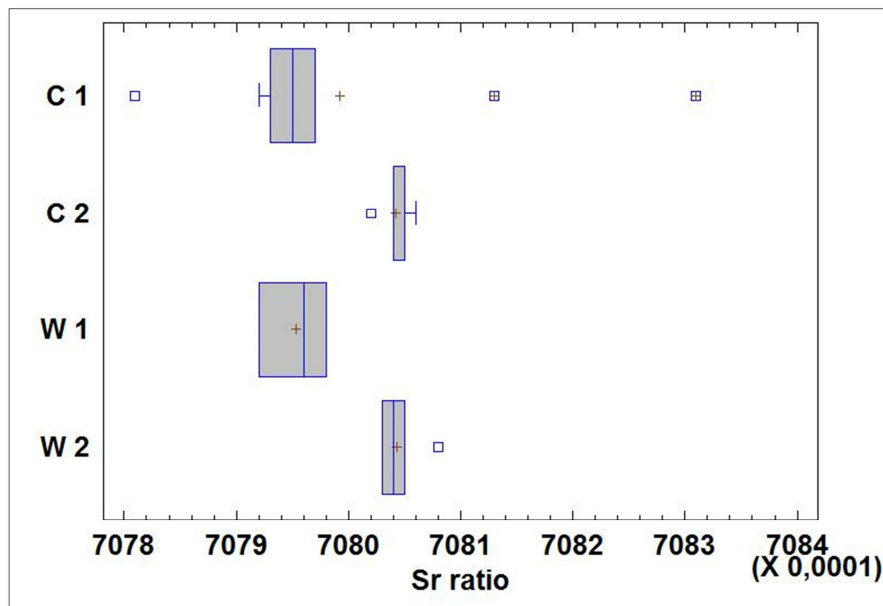


Figure 7: Box-and-Whisker plot of Sr isotope ratio values of the water (W) and carbonate sinter (C) samples of groups 1 and 2

To investigate whether the tunnel was fed only by Dafna spring, K means cluster analysis was done for the Sr isotope ratios for the carbonate sinter in the tunnel. Two clusters were found for: cluster 1 with the higher Sr isotope value of 0.7081 ± 0.00005 ; and cluster 2 with the lower Sr isotope value of 0.7077 ± 0.00005 . This means that the tunnel was fed by several sources. Ras Al Ein with the higher Sr value is located at higher altitude (620 masl) than Dafna spring (560 masl) and it could have been connected with the tunnel through open gravity channels. Qaryon spring (470 masl) is located at lower elevation.

5 Conclusions and recommendations

The Sr isotope ratios of water and carbonate sinter samples from Sebestia and Ijensinia significantly differ from those from Qaryon and Ras al Ein springs. Thus it is rather unlikely that there has been a direct connection between both water supply systems. Yet, the Sr isotope ratios of the tunnel and the aqueduct carbonate sinter samples prove that the different sources (Harun, Ijensina, Qaryon and Ras al Ein) were used to feed the water system. One may assume that additional water was needed in the area and so, more than one spring was developed. Dating the samples with e.g. the U/Th method will tell which spring was used first.

It was not possible to confirm or reject the Crowfoot theory of a linkage that existed in the past between Harun and Ijensina by using Sr isotope ratios because both springs and the carbonate sinter samples have the same Sr isotope ratio. It is clear, however, that the city Sebestia has not been linked with Nablus city via Ras Al Ein spring or Qaryon. But again it is not possible to confirm or reject the linkage between Sebestia and Nablus via Dafna spring.

So, it is recommended to repeat the geochemical analyses and to examine another isotope's ratio to prove or disprove the connection between Sebestia and Ijensinia ancient water systems. As opposed to the water network in Nablus, Ijensinia is only briefly mentioned in literature. Furthermore, what makes it hard to clearly answer the question on the connection is the fact that the spring and water system is neither excavated nor documented. Therefore, for a better understanding it is recommended to start excavations of the Ijensinia water system. So, even if the geochemical analyses lead to helpful results, they cannot replace traditional archeology.

6 Acknowledgements

This work could not have been done without the help of Nablus municipality and the department of archaeology in Nablus and Ramallah cities. They facilitated the entrance for the tunnel and the springs for samples collection. Also we wish to thank Seif Shenawy, Isam Maqbool and Salameh Shebib for the technical support during sampling.

7 List of references

- Alawi, A., Al-Masry, I., & Messerschmid, C. (2015). *Nablus Spring Source of Life Through History*. Ramallah: House of Water and Environment
- Bailey, T. R., McArthur, J. M., Prince, H., & Thirlwall, M. F. (2000). Dissolution methods for strontium isotope stratigraphy: whole rock analysis. *Chemical Geology*, 167(3–4), 313-319.
- Chancey, M. A., & Porter, A. L. (2001). The Archaeology of Roman Palestine. *Near Eastern Archaeology*, 64(4), 164-203.
- Crowfoot, J. W. b. (1966). *The buildings at Samaria, by J. W. Crowfoot, Kathleen M. Kenyon, E. L. Sukenik*. London: reprinted by Dawsons for the Palestine Exploration Fund.
- Dorale, J. A., R. L. Edwards, et al. (2004). Uranium-series dating of speleothems: current techniques, limits applications. In I. D. S. a. J. Mylroie (Ed.), *Studies of cave sediments (Physical and Chemical Records of Palesoclimate)* (pp. p. 177-197). Dordrechts: Springer.
- Fanni, I. (1999). *Nabulus fi al-hadaratayn al-Yunaniyah wa-al-Rumaniyah*. Nabulus: Baladiyat Nabulus.
- Fanni, I. (2007, March 2007). Shechem -Mamurta -Mabartha -Neapolis. *This week in Palestine*.
- Frumkin, A. (2002) The Aqueduct of Israel: The water-supply network of Samaria-Sebaste. & D. Amit, J. Patrich & Y. Hirschfeld (Vol. Ed.), (pp. 464): *Journal of Roman Archaeology Supplementary Series Number Forty-Six*.
- Li, D., Shields-Zhou, G. A., Ling, H. F., & Thirlwall, M. (2011). Dissolution methods for strontium isotope stratigraphy: Guidelines for the use of bulk carbonate and phosphorite rocks. *Chemical Geology*, 290(3-4), 133-144.
- PCBS. (2014). *Palestinians at the End of 2014*.
- PCBS. (2015a). *Localities in Nablus Governorate by Type of Locality and Population Estimates, 2007-2016*.
- PCBS. (2015b). *Needed, Supply and Consumed Quantities and Deficit in Domestic Supply in the West Bank by Governorate, 2013*.
- Raferty, C. E. R., van Bellen, R. C., & al-Markaziyah, J. S. a.-M. (1965). *Nablus District Water Resources Survey: Geological and Hydrological Report, February 1965*.
- Ruddiman, W. F. (2013). Bridging a Disciplinary Gap *Climates, Landscapes, and Civilizations* (pp. 1-10): American Geophysical Union.
- Ruppel, S. C., James, E. W., Barrick, J. E., Nowlan, G., & Uyeno, T. T. (1996). High-resolution ⁸⁷Sr/⁸⁶Sr chemostratigraphy of the Silurian: implications for event correlation and strontium flux. *Geology*, 24(9), 831-834.
- Sabri, R., Merkel, B., & Tichomirowa, M. (2015). *Urbanization effect on groundwater quality (Paleohydrogeological study)*. Paper presented at the EGU 2015.
- Spötl, C., & Matthey, D. (2006). Stable isotope microsampling of speleothems for palaeoenvironmental studies: A comparison of microdrill, micromill and laser ablation techniques. *Chemical Geology*, 235(1–2), 48-58.
- Spring water chemsity. (2011). Ramallah: Palestinian Water Authority Database department

Appendix 1: Dafna spring water quality (temperature T is in °C)

Date	Dataset	Ca mg/l	Mg mg/l	Na mg/l	K mg/l	Na+K mg/l	HCO3 mg/l	Cl mg/l	SO4 mg/l	Cl+F mg/l	TDS mg/l	pH	T
28.01.1961	Raferty 1965	90	6	27.5		29.5	231.8	62	60	62	436	7.4	
24.04.1962	Raferty 1965	72	11	21		23	209.8	44	60	44	326	7.6	
15.12.1962	Raferty 1965	74	3	16	2	18	183.0	30	11	30	280	7.4	
08.08.1963	Raferty 1965	73	4	13	1	14	176.9	34	5	34	290	7.8	
05.05.1991	Palestinian Water Authority 2011	94.5	7.5	30.5	2.1	32.6	242	50	17.5	50			
14.11.1992	Palestinian Water Authority 2011	77	7.1	25.6	1.4	27	209	48	14	48			
20.12.1993	Palestinian Water Authority 2011	91.4	7.2	29.2	1.6	30.8	245	50	15	50			
23.10.1995	Palestinian Water Authority 2011	57	5	24	1	25	130	49	10	49			
01.07.1996	Alwai 2015	114.2	6.1	32.9	3.4	36.3	221.2	94	0	94	297	7.2	
01.02.1998	Alwai 2015	73	12	52	2.6	54.6		80.4	8.5	80.4	400	7.4	
20.04.1999	Palestinian Water Authority 2011	95	7	23	1.7	24.7	240	56	14	56	268	7.1	18.6
12.10.1999	Palestinian Water Authority 2011	45	8	21	1.9	22.9	215	46		46	253	7.7	
11.04.2000	Palestinian Water Authority 2011	93	7	24	3	27	193	55	10	55	225	7.7	
28.01.2001	Palestinian Water Authority 2011	96	11	28	5.6	33.6	258	94	7	94	475	7.1	
01.07.2003	Alwai 2015	60	12.5	32.4	2.3	34.7	191	59.9	5	59.9	326	7.2	
01.06.2004	Alwai 2015	61	14.6	34.9	2.2	37.1	230	57.6	7.7	57.6	340	7.4	
01.09.2006	Alwai 2015	62	15	35	1.5	36.5	220	59.9	8	60	350	7.5	
01.08.2011	--	104.8	6.6	24.9	1.6	26.5	255.2	52.3	17.9	52.4	415	7.3	18.5

Appendix 2: Ras Al Ein spring water quality. (temperature T is in °C)

Date	Dataset	Ca mg/l	Mg mg/l	Na mg/l	K mg/l	Na+K mg/l	HCO3 mg/l	Cl mg/l	SO4 mg/l	Cl+F mg/l	TDS mg/l	pH	T
23.01.1954	Raferty 1965	68	6	8	0.5	8.5	259.86	23	5	23	323		
28.01.1961	Raferty 1965	66	6	11	0.5	11.5	239.12	24	145	24	239		
24.04.1962	Raferty 1965	76	6	10	0.5	10.5	168.36	24	51	24	245		
15.12.1962	Raferty 1965	64	6	9	0.5	9.5	195.20	16	8	16	235	7.5	
05.05.1991	Palestinian Water Authority 2011	72	2.5	10	0.3	10.3	186	20	6.5	20			
14.11.1992	Palestinian Water Authority 2011	52.6	3.3	16.5	0.4	16.9	152	22	5.5	22			
20.12.1993	Palestinian Water Authority 2011	86.2	32.3	20.1	0.5	20.6	206	34	9.5	34			
23.10.1995	Palestinian Water Authority 2011	72	8	16	1	17	244	31	5	31			
01.06.1996	Alwai 2015	78.1	2.4	24.3	0.31	24.6	244.2	49.5	0	49.5	198	7.0	
12.10.1999	Palestinian Water Authority 2011	76	10	14	0.9	14.9	201	42		42	252	8.2	20.1
11.04.2000	Palestinian Water Authority 2011	70	7	9	1	10	165	43	5	43	235	7.7	
28.01.2001	Palestinian Water Authority 2011	68	10	4	1	5	194	31	3	31	222	7.5	
01.07.2003	Alwai 2015	45	13.5	18.1	0.38	18.5	239.73	30.1	4.5	30.2	231	7.5	
01.06.2004	Alwai 2015	47	12.5	19	0.9	19.9	213.5	34	13.1	34.1	265	7.7	
01.09.2006	Alwai 2015	51	12	17	10	27	215.57	32	7	32.1	258	7.6	
01.09.2009	Alwai 2015	53	13	21	1.5	22.5	226.92	40	8	40	270	7.4	
01.08.2011		89.29	3.4	10.5	0.075	10.6	243.50	20.6	6.4	6.5	289	7.3	18.1

Appendix 3: Qaryon spring water quality. (temperature T is in °C)

Date	Dataset	Ca mg/l	Mg mg/l	Na mg/l	K mg/l	Na+K mg/l	HCO3 mg/l	Cl mg/l	SO4 mg/l	Cl+F mg/l	TDS mg/l	pH	T
02.12.1960	Raferty 1965	40	21	17	1	18	239.12	35.5	5		288	7.3	
28.01.1961	Raferty 1965	70	10	14	1	15	213.5	27	57		262	7.3	
24.04.1962	Raferty 1965	72	5	10	1	11	206.18	24	19		237	8.2	
15.12.1962	Raferty 1965	66	4	11	1	12	189.1	20	8		245	7.5	
08.08.1963	Raferty 1965	66	3	10	1	11	189.1	20	9		240	7.4	
05.05.1991	Palestinian Water Authority 2011	72.5	3.5	16	1.2	17.2	201	26	9.5	26			
14.11.1992	Palestinian Water Authority 2011	63.9	4.4	19.8	1.9	21.7	168	35	16	35			
26.12.1993	Palestinian Water Authority 2011	75.5	4.6	20.7	2.8	23.5	203	45	9.5	45			
23.10.1995	Palestinian Water Authority 2011	64	4	15	2.0	17	188	28	5	28			
01.07.1996	Alwai 2015	76.1	9.7	19.3	1.8	21.1	221.2	49.5	1	49.5	231.68	7.3	
01.02.1998	Alwai 2015	62	10.5	28	2	30.1	198	53.6	1	53.6	300	7.5	
17.05.1999	Palestinian Water Authority 2011	54	4	15	2.1	17.1	186	37	13	37	221	6.8	19.8
11.04.2000	Palestinian Water Authority 2011	71	3	13	3	16	161	27	6	27	204	7.4	
01.07.2003	Alwai 2015	57	12.9	18.6	1.45	20.1	191	39.9	5.5	40	270	7.2	
01.05.2004	Palestinian Water Authority 2011	31	29	14	1	15	185	35	12	35.1	254	7.2	19
01.09.2006	Alwai 2015	57	13.7	19.5	1.9	21.4	190	45	6	45.2	290	7.2	
01.08.2011		92.2	4.2	19.1	3.1	22.2	271.8	35.7	9.5	35.8	364.8	7.2	18.7

Appendix 4: Al Subyan spring water quality. (temperature T is in °C)

Date	Dataset	Ca mg/l	Mg mg/l	Na mg/l	K mg/l	Na+K mg/l	HCO3 mg/l	Cl mg/l	SO4 mg/l	Cl+F mg/l	TDS mg/l	pH	T
08.04.1999	Palestinian Water Authority 2011	57	21	15	1.9	16.9	237	39	12	39	289	6.8	
10.10.1999	Palestinian Water Authority 2011	33	21	26	0.7	26.7	222	62		62	287	6.8	19.4
07.05.2000	Palestinian Water Authority 2011	41	18	18	4	22	191	29	15	29	230	7.0	20
20.08.2001	Palestinian Water Authority 2011	91	21	12	3	15	239	38	3	38	286	7.4	20.5
01.08.2011		150.4	8.4	38.0	2.0	40.1	386.2	78.8	20	79.0	587	7.6	19.5

Appendix 5: Beit al ma spring water quality, (temperature T is in °C)

Date	Dataset	Ca mg/l	Mg mg/l	Na mg/l	K mg/l	Na+K mg/l	HCO3 mg/l	Cl mg/l	SO4 mg/l	Cl+F mg/l	TDS mg/l	pH	T
23.01.1954	Raferty 1965	69.16	8.41	18.00	6.0	22.4	70.2	62.00	14.64	15.12	395		
15.12.1962	Raferty 1965	63.86	6.02	44.00	6.0	30.1	70.9	88.00	4.71	24.36	510	7.3	
08.08.1963	Raferty 1965	64.54	7.80	33.00	6.0	27.7	74.3	70.00	3.21	22.45	440	7.4	
12.05.1991	Palestinian Water Authority 2011	63.10	5.17	41	5.0	31.7	74.4	61	6.6	19.1			
14.11.1992	Palestinian Water Authority 2011	62.26	6.61	34.9	4.2	31.1	71.5	62	6.0	22.5			
26.12.1993	Palestinian Water Authority 2011	63.35	6.16	37.6	5.0	30.5	74.4	60	5.5	20.1			
23.10.1995	Palestinian Water Authority 2011	57.66	8.11	33	5.0	34.2	68.9	58	5.0	26.1			
20.04.1999	Palestinian Water Authority 2011	65.79	6.23	34	6.4	28.0	66.5	93	5.4	28.1	306	7.1	
11.04.2000	Palestinian Water Authority 2011	67.52	11.11	22	3.0	21.4	66.4	70	3.8	29.8	265	7.6	
28.01.2001	Palestinian Water Authority 2011	63.57	10.08	30	4.0	26.4	76.2	59	2.2	21.6	347	7.2	
01.07.2003	Alwai 2015	52.99	20.51	28.3	2.7	26.5	69.5	69	3.7	26.9	346	7.1	
01.09.2006	Alwai 2015	54.58	16.29	32	2.7	29.1	73.1	71	3.3	23.6	390	7.2	
01.08.2011		68.67	5.50	33.73	3.6	25.8	74.4	65.7	5.4	20.2	449	7.1	19.8

Appendix 6: Zawata spring water quality. (temperature T is in °C)

Date	Dataset	Ca mg/l	Mg mg/l	Na mg/l	K mg/l	Na+K mg/l	HCO3 mg/l	Cl mg/l	SO4 mg/l	Cl+F mg/l	TDS mg/l	pH	T
19.10.1999	Palestinian Water Authority 2011	68.91	8.40	13	0.5	22.69	142	43			200		
10.04.2000	Palestinian Water Authority 2011	74.03	7.79	13	1	18.18	166	29	5		204		
01.08.2011		79.43	5.45	12.34	0.57	15.12	87.4	21.4	3.5	9.1	262		

Appendix 7: Kfar Farat spring water quality. (temperature T is in °C)

Date	Dataset	Ca mg/l	Mg mg/l	Na mg/l	K mg/l	Na+k mg/l	HCO3 mg/l	Cl mg/l	SO4 mg/l	Cl+F mg/l	TDS mg/l	pH	T
05.05.1991	Palestinian Water Authority 2011	67.5	5	17.5	1.7	19.2	208	24	8.5	24			20
19.11.1992	Palestinian Water Authority 2011	66.8	5.4	16.6	2.3	18.9	174	26	8.5	26			19
01.12.1993	Palestinian Water Authority 2011	68.1	6.5	18.5	2.2	20.7	206	27	7	27			22.5
23.10.1995	Palestinian Water Authority 2011	33	8	16	2	18	123	28	5	28			22
21.05.1997	Palestinian Water Authority 2011												
29.11.1998	Palestinian Water Authority 2011												
19.04.1999	Palestinian Water Authority 2011	52	6	20	3.6	23.6	186	46	8	46	202	7.0	20.4
12.10.1999	Palestinian Water Authority 2011	33	9	13	2.1	15.1	177	52		52	196	7.8	20.4
22.04.2000	Palestinian Water Authority 2011	68	4	15	2	17	160	36	8	36	194	6.8	20.1
01.08.2011		78.4	5.5	14.0	1.9	15.9	253.5	23.3	8.6	23.5	306	7.4	20.5

Appendix 8: Harun spring water quality. (temperature T is in °C)

Date	Dataset	Ca mg/l	Mg mg/l	Na mg/l	K mg/l	Na+K mg/l	HCO3 mg/l	Cl mg/l	SO4 mg/l	Cl+F mg/l	TDS mg/l	pH	T
27.06.1963	Raferty 1965	60	2.5	9	0.6	9.6	175.68	12	38	12	266	7.8	
30.09.1963	Raferty 1965	60	5	12	0.6	12.6	206.18	27	11	27	284	8.2	
05.05.1991	Palestinian Water Authority 2011	66.5	3	12.5	0.6	13.1	194	20	6.5	20			
19.11.1992	Palestinian Water Authority 2011	61.2	3.6	13.2	1	14.2	178	22	5.5	22			
01.12.1993	Palestinian Water Authority 2011	64.4	4.6	14.5	1	15.5	191	24	6	24			
23.10.1995	Palestinian Water Authority 2011	49	5	13	1	14	147	23	5	23			
19.04.1999	Palestinian Water Authority 2011	54	4	15	1.9	16.9	178	44	8	44	185	7.2	20.9
12.10.1999	Palestinian Water Authority 2011	39	8	11	1	12	163	42	5	42	201	7.7	20.1
10.04.2000	Palestinian Water Authority 2011	61	7	11	1	12	162	35	3	35	198	7.0	19.6
08.08.2011	--	74.9	3.7	11	0.6	11.6	234.1	20.2	6.2	20.3	278	7.4	19.8

Appendix 9: Ijnisinya spring water quality. (temperature T is in °C)

Date	Dataset	Ca mg/l	Mg mg/l	Na mg/l	K mg/l	Na+K mg/l	HCO3 mg/l	Cl mg/l	SO4 mg/l	Cl+F mg/l	TDS mg/l	pH	T
31.12.1960	Raferty 1965	86	10	25		26	334	34	35	34	464	7.6	
24.04.1962	Raferty 1965	44	5	18		19	172	24	15	24	247	7.9	
05.05.1991	Palestinian Water Authority 2011	76	5	23	0.9	23	218	28	10	28	231		20
19.11.1992	Palestinian Water Authority 2011	82	6	22	0.9	23	202	33	11	33	255		19
01.12.1993	Palestinian Water Authority 2011	67	6	25	0.8	26	198	33	9	33	247		
23.10.1995	Palestinian Water Authority 2011	56	5	25	1.0	26	174	43	7	43			
17.05.1999	Palestinian Water Authority 2011	25	6	20	1.2	21	162	30	14	30	231		20
18.11.1999	Palestinian Water Authority 2011	52	3	17	0.7	18	182	36	7	36	255		20
08.08.2011	--	90	7	19	1.1	20	282	31	10	32	1144	7.3	20

Appendix 10: Ein Al Hud spring water quality. (temperature T is in °C)

Date	Dataset	Ca mg/l	Mg mg/l	Na mg/l	K mg/l	Na+K mg/l	HCO3 mg/l	Cl mg/l	SO4 mg/l	Cl+F mg/l	TDS mg/l	pH	T
12.10.1963	Raferty 1965	56	6	23	6	29	179.34	27	38.5		305	8.4	
08.08.2002	Palestinian Water Authority 2011	77	8	23	6.1	29.1	151	37				7.8	22.5
01.08.2011	--	100.4	12	32	6	38	292	61	31	61	893	8.1	23.1

Appendix 11: Qabu spring water quality. (temperature T is in °C)

Date	Dataset	Ca mg/l	Mg mg/l	Na mg/l	K mg/l	Na+K mg/l	HCO3 mg/l	Cl mg/l	SO4 mg/l	Cl+F mg/l	TDS mg/l	pH	T
24.04.1962	Raferty 1965	58	5	30	4	34	176	52	34	52	323	7.4	
12.10.1963	Raferty 1965	52	5	32	6	38	144	41	50	41	304	8.3	
01.08.2011	--	66	7	33	1	34	156	62	15	62	1137	7.8	22